Geochemistry, Geophysics, Geosystems

RESEARCH ARTICLE
10.1029/2019GC008802

Mineralogy and Origin of Aerosol From an Arc Basaltic Eruption: Case Study of Tolbachik Volcano, Kamchatka

M. Zelenski[1], V. S. Kamenetsky[1,2], Yu. Taran[2,3], and A. M. Kovalskii[4]

[1]Institute of Experimental Mineralogy, Chernogolovka, Russia, [2]Institute of Volcanology and Seismology, Petropavlovsk-Kamchatsky, Russia, [3]Institute of Geophysics, UNAM, Ciudad de Mexico, Mexico, [4]Inorganic Nanomaterials Lab, National University of Science and Technology "MISiS", Moscow, Russia

Key Points:
- Seventy three phases were identified in Tolbachik aerosol, including droplets of H_2SO_4, silicate clasts and microspheres, and 70 minerals
- Fragmentation, alteration, and condensation aerosol are three main classes of Tolbachik aerosol particles according to their origin
- Volcanic emission of the condensation aerosol may be a noticeable factor in the redistribution of elements between geological environments

Supporting Information:
- Supporting Information S1

Correspondence to:
M. Zelenski,
volcangas@gmail.com

Citation:
Zelenski, M., Kamenetsky, V. S., Taran, Y., & Kovalskii, A. M. (2020). Mineralogy and origin of aerosol from an arc basaltic eruption: Case study of Tolbachik volcano, Kamchatka. *Geochemistry, Geophysics, Geosystems*, *21*, e2019GC008802. https://doi.org/10.1029/2019GC008802

Received 5 NOV 2019
Accepted 7 FEB 2020
Accepted article online 10 FEB 2020

Abstract Intense emission of volcanic aerosol accompanied the 2012–2013 basaltic effusive eruption of Tolbachik volcano, Kamchatka. The aerosols sampled contain sulfuric acid droplets, glassy particles, and 70 mineral phases. All aerosol particles may be classified by their origin. The fragmentation aerosol includes magma fragments: silicate glass clasts, silicate microspheres, and small phenocrysts (olivine, pyroxene, and magnetite). The alteration aerosol comprises particles of quenched silicate melt covered with secondary minerals (fluorides, sulfates, and oxides/hydroxides of rock-forming elements) and fragments of altered rocks composed solely of secondary minerals. The condensation aerosol dominated the mass during the later stages of the eruption when the explosive activity had ceased, and was characterized by the greatest variety of particle compositions. Na-K sulfate and Fe (III) oxide comprised more than 95% of the solid fraction of the condensation aerosol. The remaining 5% was represented by native elements (Au, Ag-Pt alloy, and Pt); sulfides of Fe, Cu, Ag, and Re; oxides and hydroxides of Al, Fe, Cu, Zn, Mo, W, Ta, and Zr; halides of Al, Mg, Na, K, Ca, Cd, Pb, Ag, and Tl; and sulfates of Na, K, Pb, Ca, and Ba; the only silicate was As-bearing orthoclase. Droplets of H_2SO_4 formed the liquid phase of the condensation aerosol. Some of the aerosol components, such as magnetite spherules or phosphate-carbonate-fluorite association, likely had a nonvolcanic origin (country rocks and wood fly ash). The volcanic aerosols and their contained minerals, discharged at Tolbachik and elsewhere, result in a physical and chemical effect on the environment in the region of such volcanoes.

1. Introduction

Volcanic aerosol consists of solid and liquid particles dispersed in the atmosphere that range in size from 1 nm to approximately 100 μm and originate from many forms of volcanic activity. Two processes that can form volcanic aerosol are the fragmentation of material consisting of silicate melt or solid rocks and minerals, and condensation of solid or liquid particles from the gaseous phase, including condensation of liquid particles followed by evaporation of solvent to produce aerosol of solid residue (Kondratyev et al., 2006; Mather et al., 2003; Willeke & Baron, 1993). Magmas and the host rocks of magma conduits, as well as the mineral assemblages formed during fumarolic activity or alteration processes, can be subjected to fragmentation, thus generating particles with compositions that may be similar to those of rocks. By contrast, condensation aerosol has a chemical composition that is distinctly different from those of the parent rocks and magmas. The gaseous species of volatile metals and semimetals exsolved directly from silicate melt form the aerosol particles upon cooling and condensation. The mineral composition of the condensation aerosol is diverse and may include native elements, oxides and salts of rock-forming, chalcophile and highly siderophile elements (e.g., Aiuppa et al., 2003; Mather, 2015; Mather et al., 2012; Meeker et al., 1991; Zreda-Gostynska et al., 1997).

Hotspot and rift volcanoes of basaltic composition that erupt effusively or persistently degassing lava lakes are typically quiet enough to collect aerosol samples. Previous sampling of this type of discharge includes Kilauea (Crowe et al., 1987; Darzi, 1981; Mather et al., 2012; Zoller et al., 1983), Holuhraun (Gauthier et al., 2016; Ilyinskaya et al., 2017), and Erebus (Ilyinskaya et al., 2010; Meeker et al., 1991; Zreda-Gostynska et al., 1997). Explosive eruptions of andesitic arc volcanoes are not favorable for near-vent studies of aerosols, since eruptive clouds are heavily loaded with coarse particles. Arc volcanoes with permanent or intermittent lava lakes (Masaya, Villarrica, Ambrym) or that have persistent fumarolic or open-vent degassing (e.g., Etna and Lascar) are suitable for sampling. The chemical compositions and particle size

distributions of volcanic aerosol (both fragmentation and condensation varieties) from arc volcanoes have been studied in detail, including Masaya (Martin et al., 2009; Mather et al., 2003; Moune et al., 2010), Villarrica (Mather, Tsanev, et al., 2004; Sawyer et al., 2011), Etna (Aiuppa et al., 2003; Allen et al., 2006; Mather, Oppenheimer, et al., 2004; Martin et al., 2008), and Lascar (Menard et al., 2014). Arc volcanoes of basaltic composition are rare, thus limiting opportunities to study the aerosol condensed from the nonexplosive gas emissions at the surface of a basaltic lava flow.

In parallel with studies of the general chemical composition and particle size distribution of volcanic aerosol, studies have also examined mineral assemblages. As expected, sulfates, chlorides, and fluorides of rock-forming elements, as well as particles of the silicate melt, have been identified (e.g., Varekamp et al., 1986). Crystals and aggregates composed solely of native gold were identified in aerosol from Erebus (Meeker et al., 1991), and more complex or exotic particles have been observed, including fragmented host metamorphic rocks and particles of complex unresolved compositions in the aerosol from Popocatepetl (Obenholzner et al., 2003). Arc volcanoes of basaltic composition (Tolbachik, Masaya, Villarrica, Ambrym) differ in composition of gas emissions from hotspot and rift volcanoes, both in major gas constituents such as S and HCl and in trace element composition (e.g., Edmonds et al., 2018). Therefore, one can expect major differences in mineral compositions of the condensation aerosol sampled on volcanoes from different tectonic settings. However, a systematic study of the mineral compositions of the condensation aerosol has not been conducted on any of the mentioned volcanoes.

The 2012–2013 effusive eruption of the Plosky ("Flat") Tolbachik volcano in Kamchatka was suitable for studying aerosol emissions, particularly condensation aerosol. This event was a rare case of a quiet and easily accessible long-lasting eruption of a basaltic arc volcano. Aerosol was sampled at four sites (Figures 1 and 2): on the rim of the crater with temporary lava lake (site 1), near the large skylight in the lava tube roof (site 2), from plume over an open lava flow (site 3), and from cracks in the lava tube roof (site 4). All sampling sites had different distances from the main vent, different degassing modes, different major gas species exsolved from silicate melt, and, consequently, different mineral compositions of aerosol. The main goal of the present study was to establish a detailed account of the mineral, chemical, and morphological variability of Tolbachik aerosols. To achieve this goal, we collected aerosols on filters during three sampling sessions in February, May, and July 2013. The particles trapped on the filters were studied under scanning electron microscope (SEM) equipped with energy-dispersive spectrometers (EDSs). To explain the major constituents of the particulate Tolbachik emission, we applied a simple thermodynamic model, which satisfactorily explains the major constituents of the condensation aerosol and the secondary minerals formed on the ash particles.

2. Tolbachik Eruption

Mount Plosky Tolbachik (55.82°N, 160.39°E, 3,086 m above sea level [asl]) is the southernmost active volcano of the Klyuchevskoy volcano group, located in Central Kamchatka, Russian Far East. The 2012–2013 Tolbachik eruption started on 27 November 2012, with a swarm of earthquakes accompanying moderate explosive activity on the southern slope of Plosky Tolbachik along a 5-km-long fissure stretching north to south from 2,200 to 1,500 m asl. Th effusion rate of basaltic trachyandesite lava at the beginning of the eruption exceeded 450 m^3/s (Belousov et al., 2015). Based on satellite data, Telling et al. (2015) estimated a total SO_2 emission of ~200 kt SO_2 during the complete eruption of Tolbachik, of which ~40 kt SO_2 was released during first several hours. A petrological estimate of initial S concentration based on melt inclusion data (450–630 ppm S; Plechov et al., 2015) combined with lava volume (0.55 km^3; Belousov et al., 2015) suggests a total mass of erupted SO_2 of ~1,700 kt, almost 1 order of magnitude larger than indicated by satellite measurements.

After about a week of intense effusive and explosive activity, the eruption stabilized at the lower elevation eruptive center (55.766°N, 160.318°E, 1,600 m asl). A cone started to grow, with a temporary lava lake approximately 30×50 m in size within the crater. A subsidiary crater, smaller and less active, formed on the southern slope of the initial eruptive cone. At the bottom of the cone, a lava tube formed and its length gradually increased, reaching 900 m in February 2013, and ~4 km by summer (Figure 1). Several skylights in the tube roof emitted volcanic gases loaded with aerosol (Figure 2a). From the lower end of the lava tube, lava continued to flow in a channel with intense degassing from its surface (Figure 2b). In this

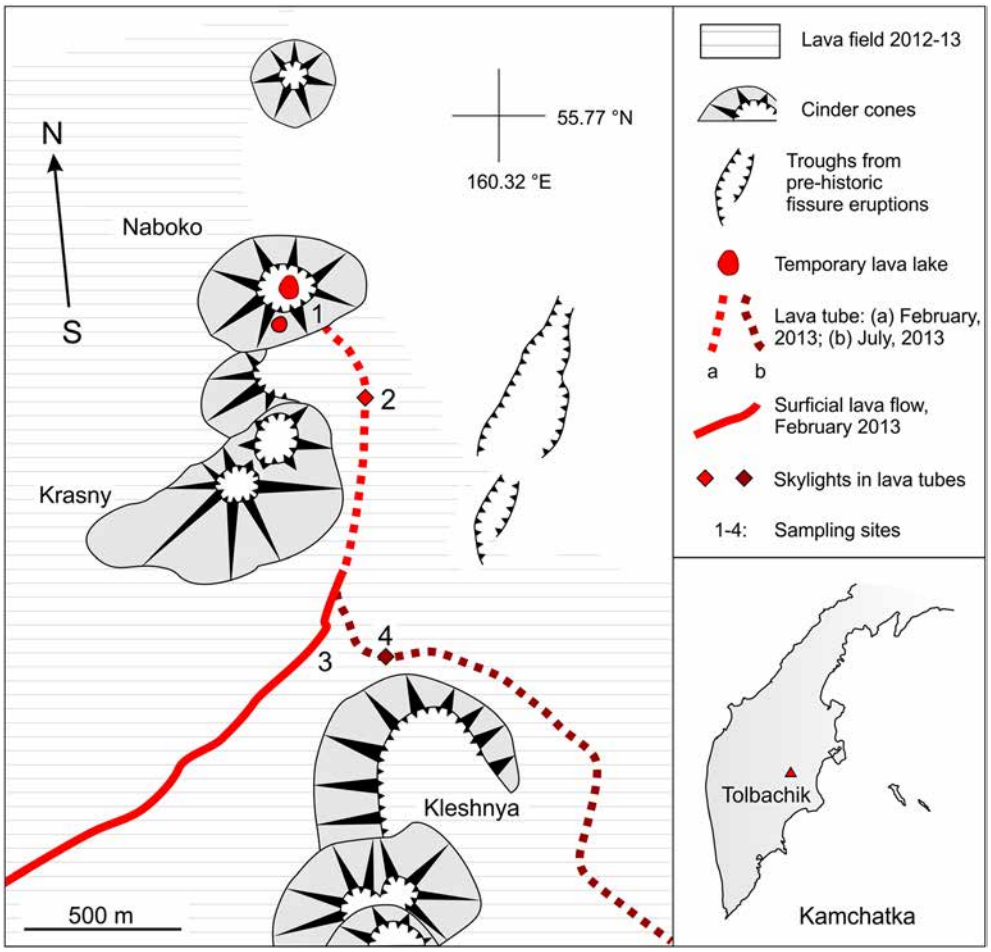

Figure 1. Scheme of the 2012–2013 Tolbachik eruption and sampling sites. Cone names: Naboko: after Sofia Naboko, Russian volcanologist; Krasny: red; Kleshnya: crab claw. Numbers denote sampling sites.

configuration, the eruption proceeded from January to August 2013, with a gradual decrease of the lava ejection rate (Belousov et al., 2015). Basaltic trachyandesite lava (most of the 0.55 km^3) and a minor amount of ash of the same composition were ejected during nine months of the eruption (Belousov et al., 2015; Volynets et al., 2015). The Tolbachik gas emissions were oxidized (H_2S content was below the detection limit of ~0.01 mol. %), contained 2–3 mol% SO_2 and up to 1.4 mol% HCl (the latter is exceptionally high for arc volcanoes; Zelenski et al., 2014). Gases emitted from the skylight in the lava tube roof contained up to 500–600 ppm total metals (Zelenski et al., 2014), the most abundant being potassium, sodium, and copper, but including the whole spectrum of chalcophile elements (Chaplygin et al., 2015; Zelenski et al., 2014).

3. Methods

We use the term "aerosol" to refer to particles with sizes ranging from several hundred nanometer to approximately 0.2 mm, the size range of the studied particles. On 26 February 2013, sampling was conducted from the plume above the upper lava tube skylight, and from the plume above a lava flow at the free surface (sites 2 and 3 respectively; Figures 1 and 2). On 3–4 May, the plume above the rim of the small crater and plume above the upper lava tube skylight were sampled (sites 1 and 2, respectively; Figures 1 and 2). On 7 July, plumes above two lava tube skylights were sampled (sites 2 and 4, respectively; Figures 1 and 2). For aerosol sampling, sterile syringe filters of 25 and 33 mm in diameter made from cellulose acetate or PTFE were used. The filter was placed at a height of 1–2 m above the ground in the area of the plume. The gas

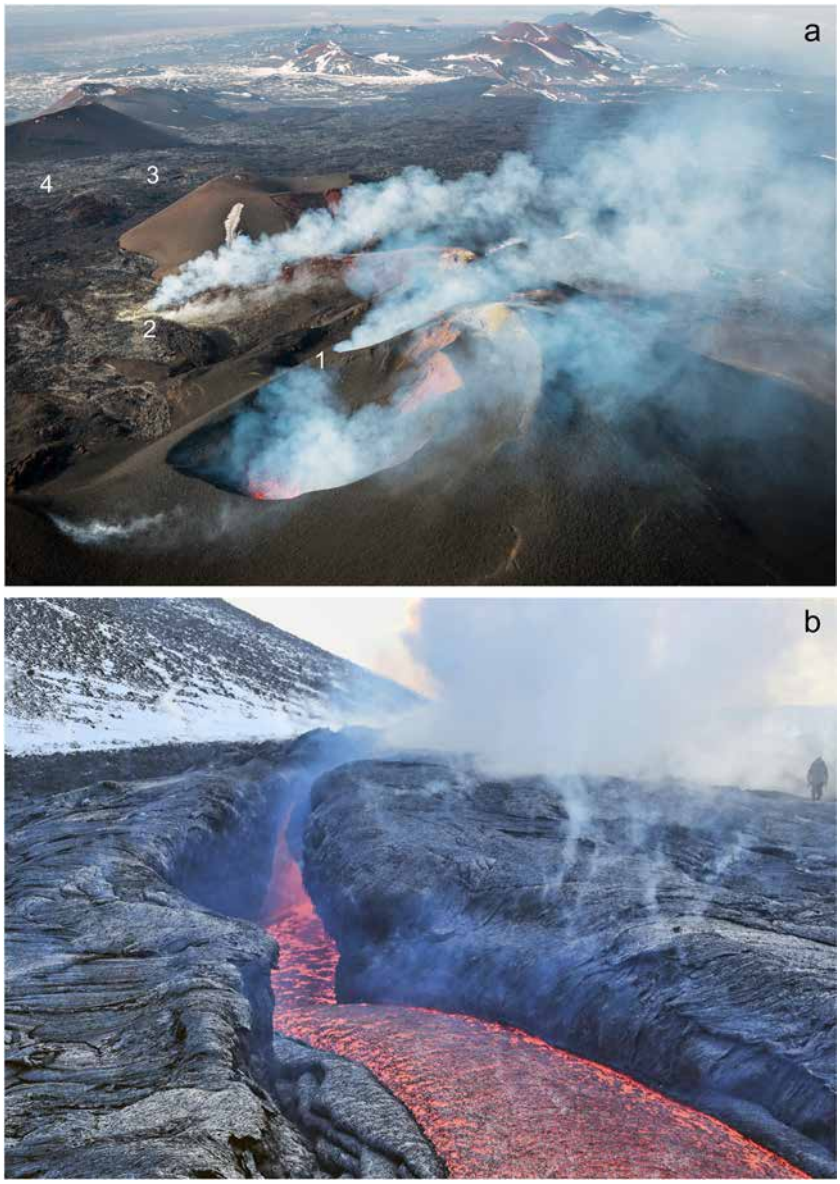

Figure 2. (a) Aerial view of intense aerosol emissions from the main and subsidiary craters on the eruptive cone and from skylights in lava tube. The 2012–2013 Tolbachik eruption, 5 May 2013. Aerial view toward the south. The eruptive cone is 110 m high. Photo by Liudmila Zemlyanskikh. (b) Plume over degassing lava flow at the surface. The blue tint of the plume (as well as in Figure 2a) is explained by Rayleigh light scattering on aerosol particles smaller than the wavelength of visible light (0.1–0.5 μm). The 2012–2013 Tolbachik eruption, 25 February 2013. Lava flow in the foreground is about 5 m wide. Numbers denote sampling sites same as in Figure 1. Photo by Vasiliy Yaschuk.

was pumped at a rate of 5–20 L/min through the filter with the flux controlled by a rotameter. The sampling process lasted approximately 30 min on average. We also separated the aerosol particles <0.2 mm from tephra around the eruptive cone using a sieve; then the heavy fraction of aerosol was separated using a heavy liquid methylene iodide with a density 3.32 g/cm^3. Simultaneously with aerosol sampling, samples were collected to determine the chemical and isotopic compositions of the Tolbachik gas emissions (Zelenski et al., 2014). A total of 24 filters were sampled.

In the laboratory, the filters were opened under sterile conditions, glued to aluminum plates and examined under a SEM with local microanalysis (Vega Tescan II XMU, IEM RAS, Chernogolovka; field emission microscope Jeol JSM 6700F, the National University of Science and Technology "MISiS," Moscow). The samples were not polished and had irregular surfaces. Therefore, the conditions of elemental analyses

were not optimal since analytical results obtained by an EDS depend on the surface angle of the specimen. In each of the analyses, we tried to locate relatively horizontal sites on a specimen and made repeated analyses to obtain average values. In most difficult cases, we took the average of two analyses of the same point on the specimen, and the second analysis was performed after the sample was rotated by 180° in the horizontal plane. In addition to the composition, crystal morphology, mineral association, and brightness of the specimen on a BSE (back-scattered electron) image, which depends on the average atomic number, were taken into account. Not all analyses could be unambiguously interpreted due to the small size of the specimen, low accuracy of the analysis on an uneven surface, and the possible presence of nonanalyzed elements (H, B, C, and N). It was difficult to interpret the mineral compositions of multiphase aggregates consisting of micron-sized crystals, as well as small crystals lying on large crystals of a different composition. Due to the adsorption of oxygen and water on the surface of the samples, the analysis of many samples showed excess oxygen contents. The filters themselves, consisting of cellulose acetate or PTFE, contain carbon, oxygen, and fluorine. Nevertheless, up to 70 solid phases were detected.

To check whether the observed mineral species in the aerosol were in equilibrium with the Tolbachik gas emissions, we performed a thermodynamic simulation of the Tolbachik aerosol system (the Outokumpu HSC 6.1 Chemistry code; Roine, 2007). The model included 12 rock-forming and volatile elements H, O, S, F, Cl, Si, Fe, Al, Na, K, Ca, and Mg and consisted of 737 species, including 275 gaseous species and 462 solid or liquid compounds. The rock-forming elements Ti and Mn as well as carbon-containing species were not included in the model for the sake of simplicity, since they play a minor role in the aerosol-forming processes. We simulated the interaction of 1 mole of Tolbachik basalt (Volynets et al., 2015) with 100 moles of the average Tolbachik gas (Zelenski et al., 2014) and 100 moles of atmospheric air, which were close to the conditions that were observed. The model calculated the temperature evolution of the gas-aerosol system from 1200 to 100°C; the total pressure was kept constant at 1 bar throughout the complete temperature range.

Microsphere sizes were manually measured on electron micrographs using a conventional vector graphics editor (CorelDraw). The size distribution was then determined using Excel Analysis Toolpack.

4. Results

All identified phases from Tolbachik aerosols are listed in Table 1. For the 2012–2013 Tolbachik eruption, the following classes of aerosol particles were identified according to their origin: (I) fragmentation aerosol, consisting of unaltered fragments of silicate melt and phenocrysts; (II) alteration aerosol, where silicate particles were altered by adsorption of gas species and subsequent leaching of elements or containing fragments of previously altered solid rocks; and (III) condensation aerosol, particles condensed from volatile metal species released directly from the magma, or high-temperature gas phase reaction products (Mather et al., 2003). Some particles could not be confidently identified and were included in an additional type (IV) for "particles of unclear origin." Below, we consider the compositions and morphologies of the Tolbachik aerosols according to this classification.

4.1. Criteria for Determining the Type of Aerosol

The origin of many aerosol particles is obvious. Silicate glass particles or small phenocrysts arise during the fragmentation of magma. Silicate glass microspheres are formed by explosions of small gas bubbles emerging at the lava surface. Particles composed entirely of secondary minerals are most likely to be formed by fragmentation of rocks that have previously undergone hydrothermal changes. Finally, sulfuric acid droplets were formed during the condensation of sulfuric acid vapor.

In two other situations, determining the origin of aerosol particles was more difficult task. On many silicate glass particles, crystals of secondary minerals containing Al, Ca, and Mg (fluorides, sulfates, and oxides) are attached. Such crystals likely formed in situ on the preexisting aerosol surfaces via alteration process. Because of extremely low volatility of Al, Ca, and Mg gaseous species in the high-temperature volcanic environment, these minerals are unlikely to have condensed from the gas. Another questionable situation is in the case of the condensation aerosol, where small single crystals and their monomineralic aggregates most likely condensed from the gas, while larger, irregularly shaped polymineral aggregates were likely fragments

Table 1
Particle Compositions of Tolbachik Aerosol According to Their Origin

#	Formula	Mineral name	Frequency*	Sampling site**	Figure #	Note
Fragmentation aerosol (types 1a and 1b)						
1	n/a	silicate glass, foam/clasts	++++	1	3a and 3b, 4a–4d, 9b, and 6a–6d	Aerosol type 1a
2	n/a	silicate glass, microspheres	++++	1, 2	4a–4d	Aerosol type 1b
3	$Ca_5(PO_4)_3(OH,Cl)$	apatite (as inclusions in magnetite)	++	1	3c	Aerosol type 1a
4	Fe $(Fe,Ti)_2O_4$	titanomagnetite	+++	1	3c	
5	$(Mg,Ca,Fe)_2Si_2O_6$	clinopyroxene	+++	1		
6	$(Mg,Fe)SiO_4$	olivine	++++	1	3d	
7	$(Na,Ca)(Al,Si)Si_2O_8$	plagioclase	+++	1		
Alteration aerosol (type II, secondary minerals)						
8	$(Al,Fe)PO_4$	unnamed	++	1, 2		
9	$AlF_3{\cdot}nH_2O$	unnamed	++	1, 2	6d and 6e	
10	AlOOH	diaspore	+++	1, 2	6f	
11	$CaSO_4$	anhydrite	+++	1, 2	6b and 6e	
12	$CaSO_4{\cdot}2H_2O$	gypsum	+++	1, 2	4c and 4d, 6c, 8k, 9b and 9c, and 11c	
13	Fe_3O_4	magnetite	+++	1, 2	6b	
14	FeOOH	goethite	+++	1, 2		
15	$(Mg,Cu,Mn)Fe_2O_4$	Cu-magnesioferrite	+	1, 2	8k	Refs. 1 and 2
16	$(Na,K)PO_4$	unnamed	++	1, 2		
17	$Na_xMg_xAl_{2-x)}(F,OH)_6{\cdot}H_2O$	ralstonite	+++	1, 2	6a	
18	NiF_2	unnamed	+	1, 2	6d	
Condensation aerosol (types IIIa and IIIb except H_2SO_4 droplets)						
19	(Ag,Tl)(Cl,Br,I)	chlorargyrite	++	2	8e	
20	Ag_2S	acanthite	++	1–4	8f, 11a, and 11c	
21	Au	gold	+++	1–4	8a and 8b and 12	Refs. 3 and 4
22	$BaSO_4$	barite	++	1, 2		
23	Cd	cadmium	+	2		
24	CuO	tenorite	++	1, 2		
25	Fe_2O_3	hematite	+++	1–3	7c and 8d	
26	Fe_2O_3	maghemite	++++	1, 2	7a	
27	Fe_3O_4	magnetite	+++	1, 2		
28	In_2O_3	unnamed	+	2	7h	
29	$(K,Na,Cu,Tl)HSO_4$	mercallite	+++	3	9a	
30	$K_2Pb(SO_4)_2$	palmierite	++	2	8d	
31	K_2SiF_6	demartinite	++	2	7c	
32	$K_3NaCu_4O_2(SO_4)_4$	wulffite	++	1, 2	8g	Ref. 5
33	$KAl_{1+x}As_xSi_3O_8$	As-bearing orthoclase	+	2	8d	
34	MoO_3	molybdite	+++	1, 2	7d	
35	$(Na,K)_2SO_4$	belomarinaite	++++	1, 2	7a and 7b	Ref. 6
36	(Na,K)Cl	halite-sylvite	++++	1, 2	8a	
37	$(Na,K,Cu,Tl)_2SO_4$	thenardite	+++	3	9a	
38	Na_2CdCl_4	unnamed	+	2	8c	
39	$NaCdCl_3$	unnamed	+	2	8c	
40	NaCl	halite	+++	1-4	8b, 8c, and 9a	
41	$NaZnCl_3$	unnamed	+	1	8h	
42	Nb_2O_5	unnamed	+	2		
43	$PbCl_2$	cotunnite	++	1, 2		
44	$PbSO_4$	anglesite	++	1, 2	8a	
45	Pd	palladium	+	2		
46	Pt	platinum	+	2, 4	11b	
47	ReS_2	rheniite	+	2	7k	
48	Se	selenium	+	2		
49	Ta_2O_5	tantite	++	1, 2	7g	
50	TeO_2	paratellurite	+	1		
51	TlI	nataliyamalikite	++	1, 2	7f	Ref. 7

Table 1
(continued)

#	Formula	Mineral name	Frequency*	Sampling site**	Figure #	Note
52	WO_3	krasnogorite	+	1, 2		
53	ZnO	zincite	+	1, 2		
54	$ZrO(OH)_2$	unnamed	++	1, 2	7e	
55	Ni,Cu,Zn,Sn,(SO4),Cl, etc.	unidentified sulfates and chlorides	+++	1–4	8h	
56	H_2SO_4	sulfuric acid	++++	1–4	Traces of acid exposure are shown in Figures 9a–9c	Aerosol type IIIc
Particles of unclear or nonvolcanic origin						
57	$CaCO_3$	calcite	++	1	12	
58	CaF_2	fluorite	++	4	11b, 11c, and 12	
59	$Ca_5(PO_4)_3F$	fluorapatite	++	4	11a, 11b, and 12	
60	$CaTiSiO_5$	titanite	+	1		
61	$Cu_{1.8}S$	digenite	+	1	10b	
62	Ag,Pt	native silver-platinum alloy	++	4	10e	
63	Ca_2PO_4Cl	chlor-spodiosite, goryainovite	++	4	11d	Ref. 8
64	Fe	native iron	+	4	12	
65	FeS_2	pyrite	+++	1	10a	
66	$FeWO_4$	ferberite	+	1	10d	
67	$K_2Ca(CO_3)_2$	fairchildite	+	4		
68	$(Na,K)_{1-x}Ca_xAlS_{3-x}O_8$	feldspar	++	4	11a	
69	magnetite (spherules)	magnetite	+++	1–3	10f	Refs. 9 and 10
70	NiO	bunsenite	+	1	10c	
71	$Ni(Fe,Ti)_2O_4$	trevorite	+	1	10c	
72	$Na_2Ca4(CO_3)_5$	Na-Ca carbonate	++	4	12	
73	$ZrSiO_4$	zircon	++	1-4		

Note.
*Frequency: + extremely rare, 1-3 particles were detected on all filters; ++ rare, 3–20 particles; +++ common, > 20 particles but <1wt. %; ++++ major phase, >1 wt. %. **Sampling locations are according to the scheme in Figure 1: 1: crater rim; 2: large skylight in the lava tube; 3: lava flow with free surface; 4: cracks in the lava tube roof.
References: 1: Kamenetsky et al., 2019; 2: Sharygin et al., 2018; 3: Zelenski et al., 2016; 4: Chaplygin et al., 2015; 5: Pekov et al., 2014; 6: Filatov et al., 2018; 7: Okrugin et al., 2017; 8: Ivanyuk et al., 2017; 9: Groves et al., 1987; 10: Srinivasachar et al., 1990. Magnetite (Fe_3O_4) appears in four different classes of aerosol.

of previously precipitated and subsequently fragmented sublimates. The latter situation is discussed in detail in section 5.1.

4.2. Particles Derived From Fragmentation of Melt and Altered Rocks

These types of aerosol are similar in cationic composition to the initial magma and may differ only in the presence of volatile elements creating anions. The fragmentation aerosol, according to our classification (types Ia and Ib), forms during fragmentation of magma, whereas "alteration aerosol" (type II) formed during fragmentation of altered rocks or alteration of silicate particles.

4.2.1. Aerosol Type Ia: Magma Fragmentation: Fine Volcanic Ash and Ablated Phenocrysts

By the time the aerosols were sampled (3 months after the start of the eruption), the Tolbachik eruption had become a relatively quiet lava effusion with almost constant ejection rate of lava and sporadic explosions in the lava lake inside the crater. A stable system of lava tubes with skylights had already formed. Judging by the visual assessment of the amount of silicate and nonsilicate particles on the filters, the fine silicate material resulting from explosive activity and the silicate microspheres arising from the bursts of small gas bubbles accounted for less than 50% of aerosol by mass.

The fragmentation of silicate magma occurs in several ways, thus providing aerosol of various compositions and sizes. Bursts of large high-density gas slugs on the magma surface result in significant velocities (up to 300–500 m/s) for lava fragments (Bombrun et al., 2015). This process of aerosol formation is likely the most productive during the period of high explosive activity. Larger fractions of pyroclastics, such as ash, lapilli, and volcanic bombs, are also formed under these conditions. Particles of the explosion-derived aerosol

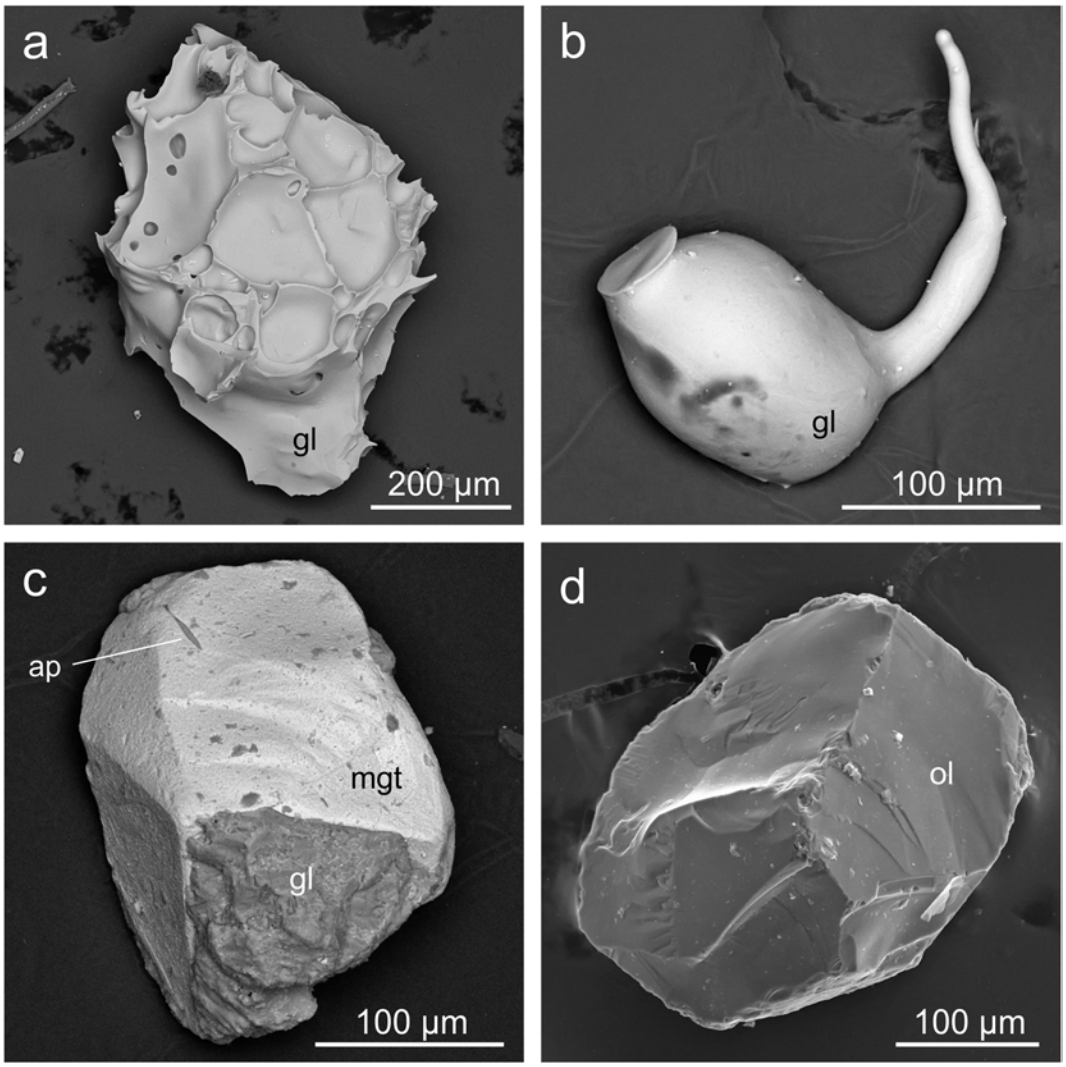

Figure 3. Aerosol particles formed by magma fragmentation. (a and b) Glass particles; (c and d), phenocrysts of major minerals. (a) Vesicular particle of silicate glass (gl) foam. (b) Elliptical glass droplet with a "tail." (c) Magnetite (mgt) crystal with remnants of silicate glass and an apatite (ap) inclusion. (d) Olivine (ol) crystal with broken surfaces possibly resulting from breakdown caused by thermal shock. (a, b, and d) Secondary electron (SE) images; (c) backscattered electron image.

were studied on filters and in the fine ash fraction. Such particles are mainly composed of quenched silicate melt (glass; Figures 3a and 3b), but small crystals of rock-forming minerals such as olivine (Figure 3d), clinopyroxene, plagioclase,and magnetite (Figure 3c) are also present. Such crystals are partially or completely devoid of silicate glass since the glass-precursor melt was ablated by the oncoming air flow when particles with high velocities flew apart from the point of explosion. The fragments of crystals with freshly exposed breakage surfaces that are common likely formed as a result of the effect of thermal shock on the crystals upon quenching or because of mechanical forces. The observed increase in the velocities of the magma fragments with a decrease in the fragment size (Bombrun et al., 2015) indicates that explosions with sufficient energy are able to extract the smallest solid objects (phenocrysts) present in the magma and to clear them from traces of the melt.

4.2.2. Aerosol Type Ib: Silicate Microspheres

A different fragmentation involving the bursting of small and low-density bubbles on the surface of the lava produces silicate microspheres, which were found to be abundant in the Tolbachik aerosol. Such microspheres are present in aerosol from the lava tube skylights (Figure 4) but also occur in aerosol samples from the plume above the eruptive crater. Similar particles have been described in aerosols from the basaltic

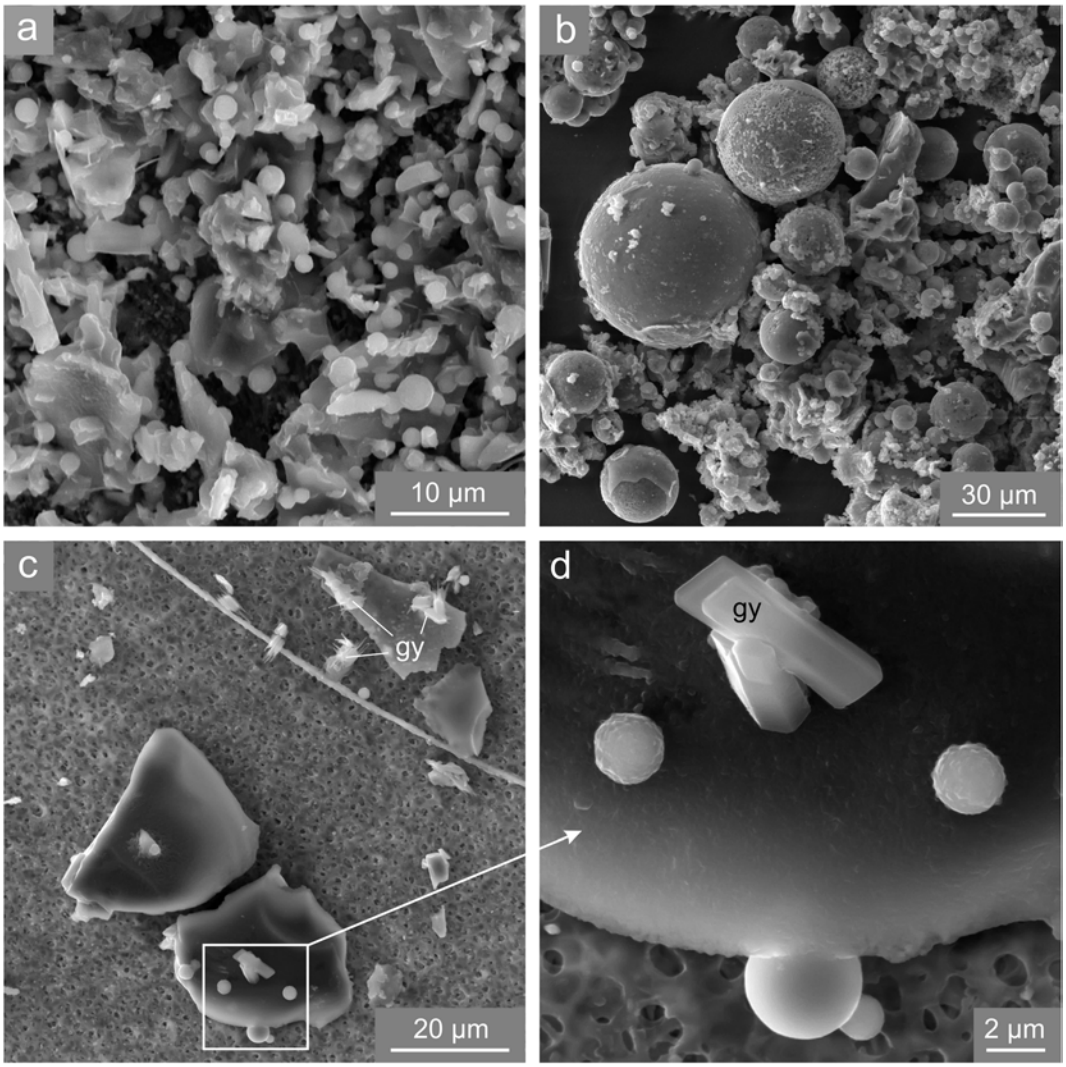

Figure 4. Silicate microspheres. (a) Monodisperse (1.6±0.5 μm) silicate glass microspheres together with dominant angular ash particles. (b) 1–60 μm silicate glass microspheres, together with altered ash particles. (c) Angular ash particles, Pele's hair, silicate glass microspheres and gypsum (gy) crystals. (d) Enlarged fragment of (c) with gypsum crystals and silicate glass microspheres: the surface of glass microspheres can be smooth (fresh) or reticulated (altered). Secondary electron images.

volcanoes Etna (Lefèvre et al., 1986; Martin et al., 2008), Kilauea (Meeker & Hinkley, 1993), Masaya (Martin et al., 2009, 2012; Moune et al., 2010), and Villarrica (Sawyer et al., 2011). Tolbachik silicate microspheres have a log-normal size distribution with two modes at 1.6 and 6.4 μm, with most microspheres of smaller size (Figure 5). Martin et al. (2008) observed a similar size distribution for silicate microspheres in Etna aerosols with a modal diameter of 1.4 μm. Bimodal size distribution can be explained by the existence of two different mechanisms for droplet formation during bubble bursting. Numerous small droplets form by film rupture, whereas few larger droplets appear as a result of cavity collapse after bursting (Martin et al., 2008, and references therein). Particularly favorable conditions for the formation of silicate microspheres exist inside the nearly isothermal lava tubes, since lava does not cool from the surface and is not covered by a crust with higher viscosity.

Unlike in the Etna aerosols, silicate microspheres were not the dominant fraction among the Tolbachik silicate aerosol. They represent less than 20–30% of the silicate aerosol, whereas the remaining silicate particles were angular clasts (Figures 4a–4c). Silicate microspheres, as well as micron-sized angular clasts, are enriched in sulfur (1–6 wt. % S) and alkali metals (up to 13.5 wt. % $Na_2O + K_2O$), but there is no significant correlation between the abundances of these elements. There is also no noticeable difference in the

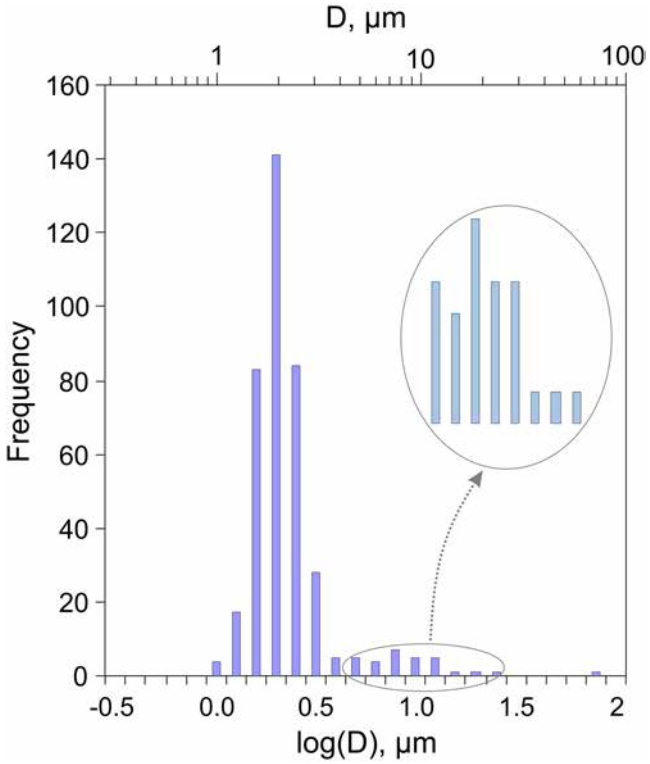

Figure 5. Bimodal log-normal distribution of the diameter of silicate microspheres in the Tolbachik aerosol.

compositions of microspheres and larger angular particles. The latter, most likely, indicates that the microspheres and the angular glass fragments have the same origin (melt fragmentation during explosions of small bubbles) but seemingly different quenching conditions.

4.2.3. Aerosol Type II: Altered Basaltic Particles and Fragments of Altered Basaltic Rocks

Two other mechanisms of aerosol formation mentioned by Mather et al. (2003) were widely present during the Tolbachik eruption: leaching/alteration of silicate aerosol and leaching/alteration of volcanic rocks followed by fragmentation. These two cases are similar; therefore, we combined the particles resulting from these two processes under the common name "alteration aerosol." They differ, however, in the sequence of the formation processes and their locations. Specifically, alteration occurs directly on aerosol particles suspended in the gas or on solid rocks followed by fragmentation. The particles formed by these two processes mainly differ in their morphologies and abundances of secondary minerals.

The altered aerosol (fragmentation first) is represented by silicate glass particles coated from the surface with separate crystals or a thin layer of secondary minerals (Figures 6a–6c). Alteration of the surface layer of silicate particles, including microspheres, occurs while they are suspended inside a lava tube, which is filled by volcanic gas plus air at a temperature ~1065°C. The time required for silicate microspheres to move from the lava surface to the skylight can be roughly estimated from the size of the lava tube (5–10 m across and about 1 km long from the source) and gas flux from the skylight (approximately 10–20 m^3/s). This results in a residence time of the gas in the lava tube from several seconds to several minutes. Previously, Spadaro et al. (2002) showed that in the presence of volcanic gases, even at ambient atmospheric temperature, cations are gradually leached out of basalt glass, which leads to a change in the glass composition.

The altered rock particles (alteration first) consist entirely of secondary minerals (e.g., Figure 6f). The list of secondary minerals (Table 1 and Figure 6) includes simple and complex aluminum fluorides (unnamed mineral $AlF_3 \cdot nH_2O$, ralstonite $Na_xMg_xAl_{2-x}[F,OH]_6 \cdot H_2O$), calcium sulfates (gypsum $CaSO_4 \cdot 2H_2O$, anhydrite $CaSO_4$), and various aluminum and iron oxides and hydroxides. In one of the fluoride-rich particles studied, a noticeable amount of NiF_2 was measured (Figure 6d). Phosphates such as $(Na,K)_3PO_3$ and $(Al,Fe)PO_3$ were observed on filters in the form of micron-sized irregular particles. The presence of secondary minerals in volcanic aerosol, as well as the presence of fragmented sublimates (section 4.2.2), is one of the main factors preventing accurate measurements of trace elements transported by volcanic gases in the gaseous form (Aiuppa et al., 2003; Zelenski et al., 2014; Zoller et al., 1983).

4.3. Particles Derived From Gas Condensation

Particles derived from gas condensation are an essential component of volcanic aerosols, if not by mass then by geochemical significance. Condensation aerosol determines the enrichment of the volcanic plumes with relatively volatile heavy elements with low concentrations (e.g., Mo, Cd, As, Ag, and Pb). Within our classification, we identified three subtypes of condensation aerosol based on morphological characteristics: IIIa—solid particles that condense from the gaseous phase, IIIb—minerals and aggregates condensed from gases on a solid surface (volcanic sublimates) and subsequently detached from the surface and fragmented into aerosol particles, and IIIc—liquid droplets condensed from the gaseous phase.

4.3.1. Aerosol Type IIIa: Solid Particles That Condense From the Gaseous Phase

Volatile metal compounds released directly from the silicate melt as well as compounds formed due to gas-phase reactions (e.g., oxidation of volcanic gas by atmospheric oxygen) can condense upon cooling to form aerosols. This class of aerosol particles (together with class IIIb—fragmented sublimates) is characterized by the greatest variety of mineral and chemical compositions. The three most abundant nonsilicate phases

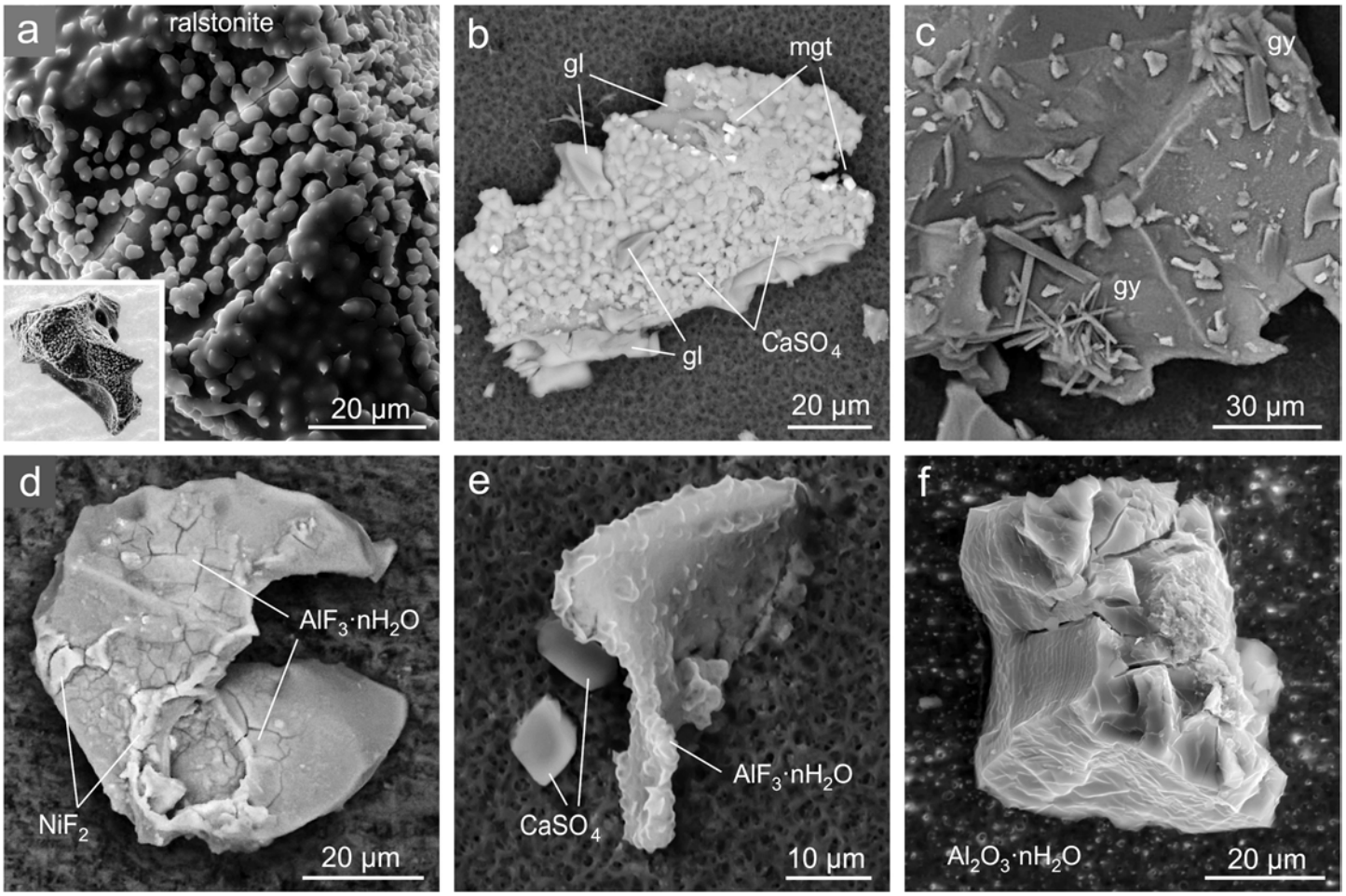

Figure 6. Aerosol particles containing secondary minerals. (a–d) Altered ash: silicate glass particles covered with secondary minerals; (e and f) secondary minerals. (a) Globules of ralstonite $NaxMgxAl_2{-}x(F, OH)_6{\cdot}H_2O$. (b) Crystals of anhydrite, $CaSO_4$, and magnetite. (c) Crystals of gypsum, $CaSO_4{\cdot}2H_2O$. (d) Thin layer of unidentified aluminum fluoride and nickel fluoride. (e) Particle of aluminum fluoride and anhydrite crystals. (f) Particle of aluminum hydroxide. (a, e, and f) Secondary electron images; (b–d) backscattered electron images. gl: silicate glass, mgt: magnetite, gy: gypsum. These phases were also observed in fumarolic incrustations at Surtsey, Eldfell, and Hekla volcanoes, Iceland (Jakobsson et al., 2008).

in the Tolbachik aerosol emissions were Na-K double sulfate, iron (III) oxide, and sulfuric acid; all three were products of the gas-phase oxidation (see Discussion). Unlike condensation aerosol studied in the Popocatepetl plume and presented mainly by spherical and fluffy particles (Obenholzner et al., 2003), condensation in the Tolbachik gases mainly resulted in well-shaped micron-sized crystals (Figure 7). Many aerosol particles of this type were individual single crystals (Figures 7a–7c), although many others, especially those containing heavy elements, were present as aggregates of tiny individual crystals (Figures 7d–7f).

Na-K double sulfate are crystals of 0.5–2.5 μm in size (Figures 7a and 7b). The atomic ratio of Na:K is close to unity. Most sulfate crystals have poorly expressed faces or have a shape close to spherical, which can be an indirect sign of condensation of liquid sulfate droplets followed by crystallization of such droplets (see Discussion). Fe (III) oxide crystals in the aerosols are represented by cubic polymorph maghemite, 2–5 μm in size and with well-defined crystal faces that are commonly flattened to thin plates (Figure 7a). Other iron oxides, magnetite Fe_3O_4 and hematite Fe_2O_3, were less common in aerosol, although they are abundant in Tolbachik sublimates (e.g., Vergasova & Filatov, 2012). In addition to $(Na,K)SO_4$ and Fe_2O_3, the Tolbachik aerosol contained other condensed phases in low abundance. Crystals and aggregates of potassium hexafluorosilicate demartinite K_2SiF_6 (Figure 7c), which was determined by its chemical composition and hexagonal bipyramidal crystal shape (Gramaccioli & Campostrini, 2007), occur in small quantities.

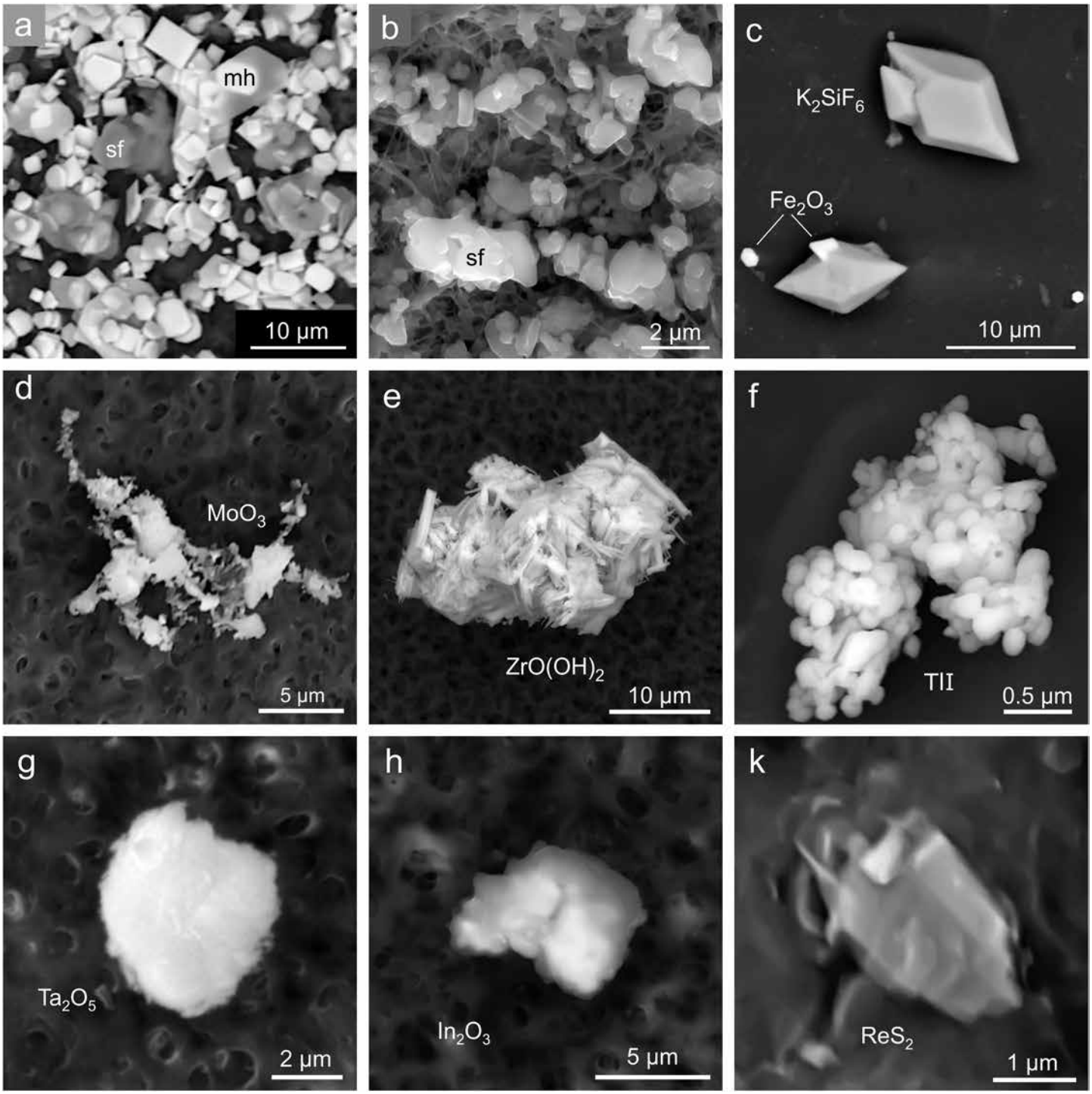

Figure 7. Examples of condensation aerosol. Particles are micron-sized individual crystals or aggregates with a visible crystalline texture. (a) Crystals of maghemite Fe_2O_3 (light) together with a smaller amount of Na-K sulfate (dark gray). Maghemite is a modification of Fe (III) oxide with cubic crystals. (b) Crystals of Na-K sulfate; many have a rounded shape. (c) Well-shaped crystals of demartinite (hexagonal modification of K_2SiF_6). (d) Fractal-like aggregated crystals of molybdenum oxide MoO_3. (e) Aggregate of acicular and sheaf-like crystals of zirconium oxide-hydroxide ZrO $(OH)_2$. (f) Aggregate of thallium iodide TlI; individual crystals are 100-200 nm in size. (g) Aggregate of Ta_2O_5. (h) Aggregate of In_2O_3 containing 1 wt. % Au. (k) Crystal of ReS_2. mh: maghemite, sf: Na-K sulfate.

Single crystals of Na-K chloride in aerosol are rare, but crystal aggregates of (Na,K)Cl are more common, which seemingly indicates the deposition of the minerals on solid rocks at lower temperatures, followed by fragmentation (section 4.2.2.).

Rare or solitary crystals and aggregates containing heavy elements were also captured by the filters. Such particles, even very small ones, are clearly visible by SEM in the phase-contrast viewing mode. The list of phases with heavy elements includes molybdenum oxide MoO_3 (Figure 7d), zirconium hydroxide oxide (Zr,Hf)O $(OH)_2$ (Figure 7e), thallium iodide TlI (Figure 7f), tantalum oxide Ta_2O_5 (Figure 7g), indium oxide In_2O_3 (Figure 7h), rhenium disulfide ReS_2 (Figure 7k), barium sulfate $BaSO_4$ (barite), silver chloride and silver sulfide, lead chloride $PbCl_2$, lead sulfates $PbSO_4$ and $K_2Pb(SO_4)_2$, and numerous micron and submicron gold particles (Table 1). Many of these phases were previously described within fumarolic incrustations at Tolbachik (e.g., Vergasova & Filatov, 2012) as well as on other volcanoes (Balić-Žunić et al., 2016). Other phases such as Ta_2O_5 has not been observed in the fumarolic environment, or, in the case of In_2O_3 and ZrO $(OH)_2$, do not correspond to the list of known minerals.

4.3.2. Aerosol Type IIIb: Fragmented Sublimates

Mineral aggregates precipitated directly from volcanic or fumarolic gases on the surface of rocks are traditionally called volcanic sublimates. Such sublimates form inside and around cracks in lava or on crater walls and can become airborne after fragmentation to form aerosol particles (for example, propelled away by a sudden increase in gas flux). Fragmented sublimates differ from aerosol gas-condensed particles. They have a relatively large size (50–200 μm), irregular or angular shape of clasts and, as a rule, polymineral compositions (section 5.1). Most of the minerals from these particles have been previously described for the fumaroles of Tolbachik or other volcanoes (Table 1). The main phases of fragmented sublimates are Na-K chloride (Figure 8a) or pure NaCl (Figure 8b) and a complex Cu-K-Na sulfate wulffite $K_3NaCu_4O_2(SO_4)_4$ (Figure 8g). The list of rare minerals among this class of aerosol particles includes two Cd-Na chlorides $NaCdCl_3$ and Na_2CdCl_4 with different Na:Cd ratios and different shapes of crystals (Figure 8b), cotunnite $PbCl_2$, anglesite $PbSO_4$ (Figure 8a), palmierite $K_2Pb(SO_4)_2$ (Figure 8d), As-bearing orthoclase $KAl_{1+x}As_xSi_3O_8$ (Figure 8d), tenorite CuO, hematite Fe_2O_3 (Figure 8d), $NaZnCl_3$ (Figure 8h), and Cu-bearing magnesioferrite $(Mg,Cu,Mn)Fe_2O_4$ (Figure 8k). Fine gold scattered everywhere is one of the remarkable features of such particles. Gold is present as individual crystals <1 μm in size (Figure 8a) or as aggregates (Figure 8b). Unlike gold, silver minerals are rarely found on volcanoes (Li & Boudreau, 2019). However, the Tolbachik aerosol contains a noticeable amount of crystals or aggregates of acanthite Ag_2S (Figure 8f) and chlorargyrite (Ag,Tl)(Cl,Br,I) (Figure 8e). In the latter case, chlorine dominates, but bromine and especially iodine are also present in appreciable amounts. Silver in such aggregates was partially replaced by thallium. Aerosol type IIIb (precipitation of sublimates followed by fragmentation) was not previously listed among processes contributing to particle formation in volcanic aerosol (e.g., review by Mather et al., 2003).

4.3.3. Aerosol Type IIIc: Liquid Particles Condensing in the Gaseous Phase

Along with solid phases, the Tolbachik aerosol contained droplets of sulfuric acid. Our methods (sampling onto simple single filters) allowed us to indirectly identify the presence of liquid aerosol particles. Some filters did not contain primary aerosol particles; instead, they were covered by phases evidently crystallized from an aqueous solution (Figure 9a). This filter was used for the collection of aerosol from the plume over the open lava flow (Figure 2b). The phases on such filters included halite, thenardite $(Na,K,Cu,Tl)_2SO_4$, and the rare mineral mercallite $(K,Na,Cu,Tl)HSO_4$, which is an acid salt (potassium bisulfate). As is known from general chemistry, the crystallization of potassium bisulfate requires free sulfuric acid in the solution. Theoretically, sulfuric acid could form in situ on the filter due to oxidation of the SO_2 dissolved in water, which can be fast in the presence of heavy metals such as Cu and Tl (Huie, 1986; Pollard et al., 1961, and references therein).

Other filters contain stronger evidence of the presence of sulfuric acid droplets. For example, Ca-rich aerosol particles (apatite, fluorite, and silicate glass) were surrounded by gypsum satellite rings (Figure 9b) or gypsum tentacle-like aggregates (Figures 9c and 11c). Some of these filter samples were collected in July 2013, in dry and warm weather in the absence of visible vapor plumes that consist of water droplets. In particular, the aerosol particles (Figures 9b, 9c, and 11c) were sampled from blue transparent fumes over a skylight at 110°C; this temperature excludes condensation of liquid water and oxidation of SO_2 directly on filters in water solution did not occur. The presence of sulfuric acid droplets in near-vent volcanic aerosols has been previously confirmed (e.g., Allen et al., 2000; Martin et al., 2008). In particular, sulfate aerosols were recorded near lava fountains and over cooling lava flows (Ilyinskaya et al., 2012). Hence, sulfuric acid droplets were most likely present in the Tolbachik aerosols.

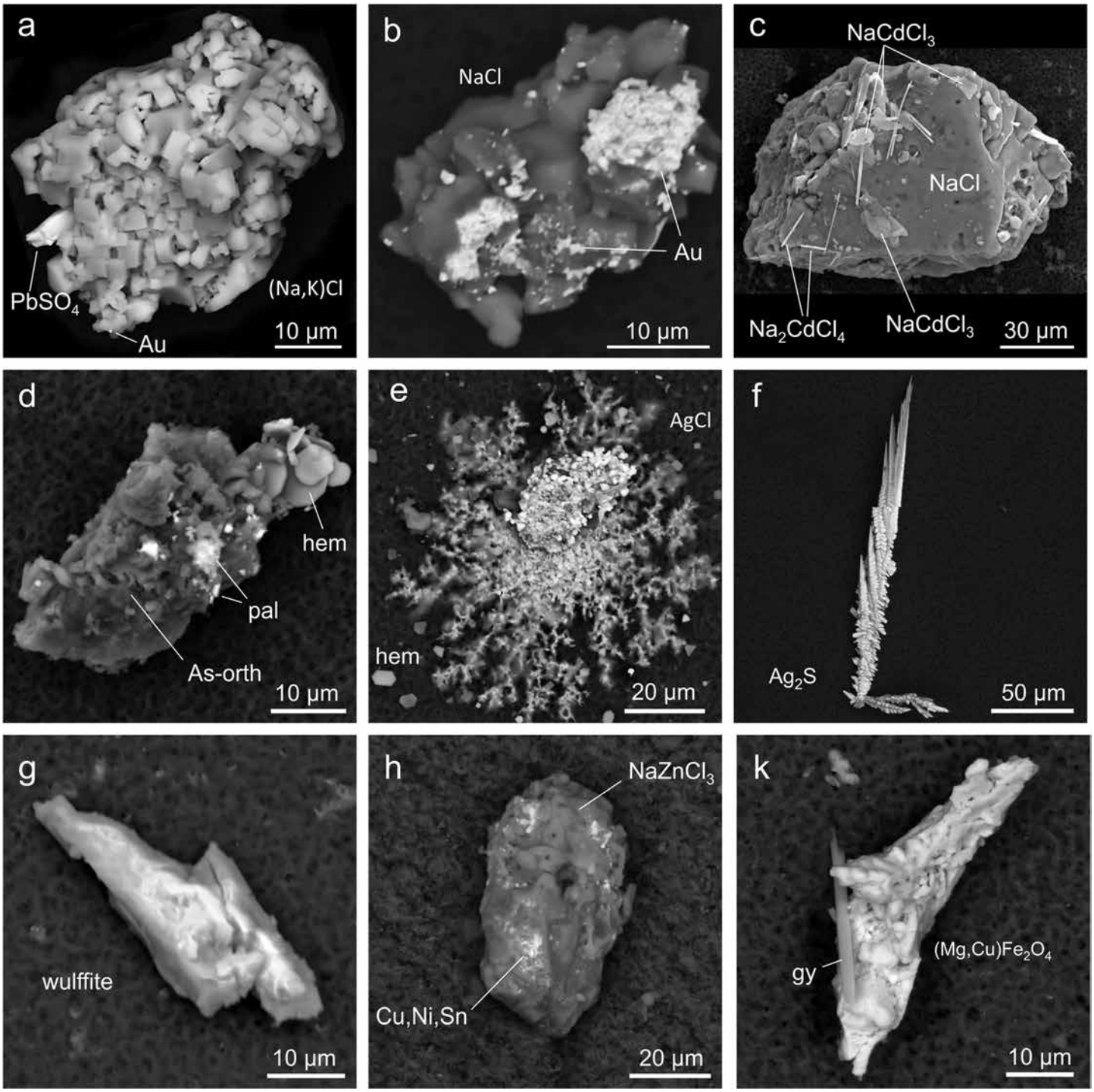

Figure 8. Aerosol particles likely formed by fragmentation of volcanic sublimates. (a) Aggregate of (Na,K)Cl crystals with Na:K ratio close to unity. The aggregate also contains anglesite $PbSO_4$ and native gold. (b) Aggregate of small gold crystals together with halite NaCl. (c) Massive halite aggregate and two Cd-Na chlorides with different Cd:Na ratios. (d) Aggregate of filatovite (As-bearing orthoclase, As-orth), palmierite, $K_2Pb(SO_4)_2$ (pal) and hematite, Fe_2O_3 (hem). (e) Aggregate of chlorargyrite (Ag,Tl)(Cl,Br,I) containing trace Br, I, and Tl. Dendrite-like halo of the same composition formed on the filter around the primary aerosol particle, suggesting the filter was wetted by an acid mixture, enriched in HCl and containing HBr and HI. (f) Monomineralic aggregate of acanthite, Ag_2S. (g) Aggregate of wulffite, $K_3NaCu_4O_2(SO_4)_4$. (h) Aggregate of $NaZnCl_3$ with unidentified inclusions of Cu, Ni and Sn sulfates or chlorides. (k) Aggregate of Cu-bearing spinel, $(Mg,Cu,Mn)Fe_2O_4$, and a gypsum crystal.

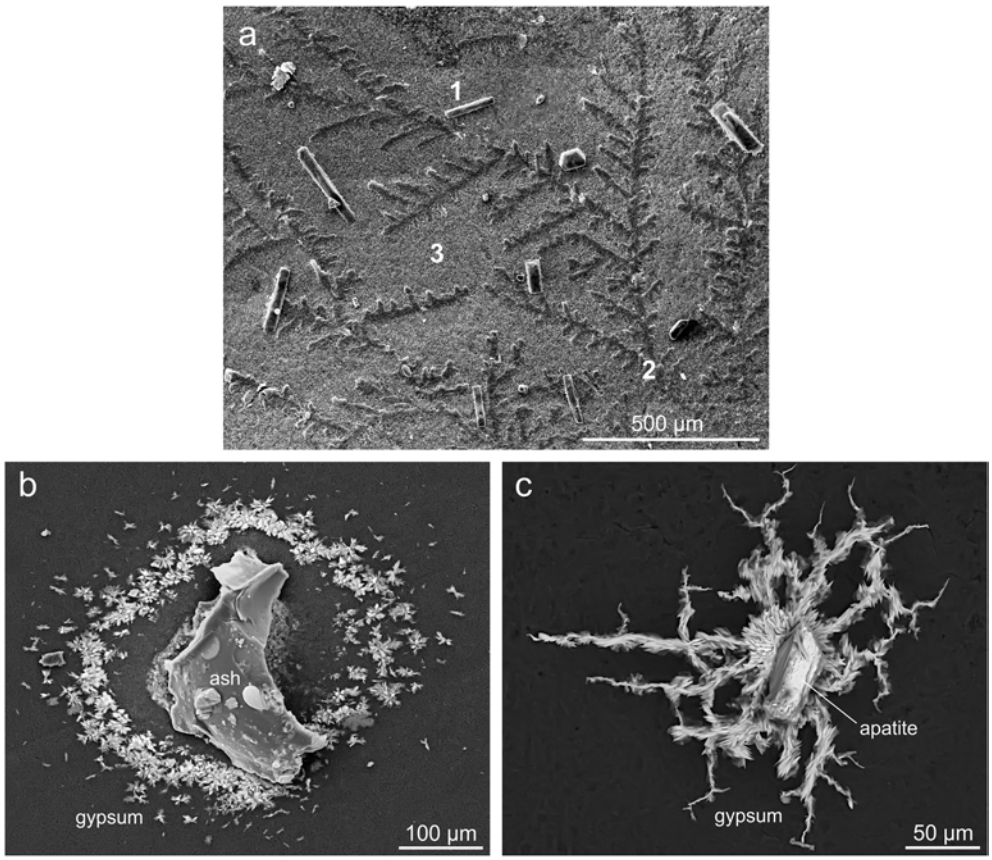

Figure 9. Evidence for sulfuric acid aerosol in aerosol samples. (a) Filter covered with crystals apparently crystallized from solution containing sulfuric acid. The filter contains (1) crystals of potassium bisulfate mercallite (K,Na,Cu,Tl)HSO_4, (2) dendrites of thenardite $(Na,K,Cu,Tl)_2SO_4$, and (3) balance of filter covered with a mixture of thenardite and halite. Potassium bisulfate (mercallite) crystallized from acid solution containing free H_2SO_4. (b) Satellite ring composed of gypsum crystals around large ash particle. (c) Tentacle-like aggregates of gypsum growing from apatite crystal. A Ca-rich particle was trapped by the filter together with droplets of sulfuric acid. Under the influence of acid, cations were leached from the particle, of which only Ca forms insoluble sulfates (gypsum). During storage, sulfuric acid gradually evaporated from the filter, leaving aggregates of secondary minerals with characteristic shapes.

4.4. Aerosol Type IV: Particles of Unclear or Nonvolcanic Origin

Above we describe particles with origins that were not difficult to determine. Based on morphology and chemical composition, we concluded that most aerosol particles in Tolbachik originated either as a result of the fragmentation of magma, fragmentation of altered volcanic rocks, or condensation from the gaseous phase (see also section 5.1). The origin of some other particles captured on filters was not as obvious. Some of the particles have the characteristic features of two or more types of aerosols or signs of extraneous (nonvolcanic) origin. We combine these as "particles of unclear origin" and discuss various possible ways of forming such particles below.

1. Pyrite (FeS_2) was present in the aerosol as crystal fragments (Figure 10a), well-shaped crystals, and aggregates. Another sulfide mineral present was a small 4-μm roundish particle of $Cu_{1.8}S$ (Figure 10b). This chemical composition is that of digenite. It is not possible to determine the exact origin and initial composition of the sulfide, since the Cu-S system is rather complex and the most stable composition depends on temperature (e.g., Cook, 1972). This sulfide may have formed at depth in a hydrothermal vein and subsequently expelled by magma or gas discharge. Its rounded shape appears due to melting rather than to erosion, because meting point of digenite (1050°C; Cook, 1972) is slightly below lava temperature (1065 °C). A relatively large (~10×40 μm) crystal of ferberite $FeWO_4$ (Figure 10c) contains 2 wt. % Re. An aggregate of octahedral crystals of trevorite (Ni $(Fe,Ti)_2O_4$) together with bunsenite NiO was found on a filter

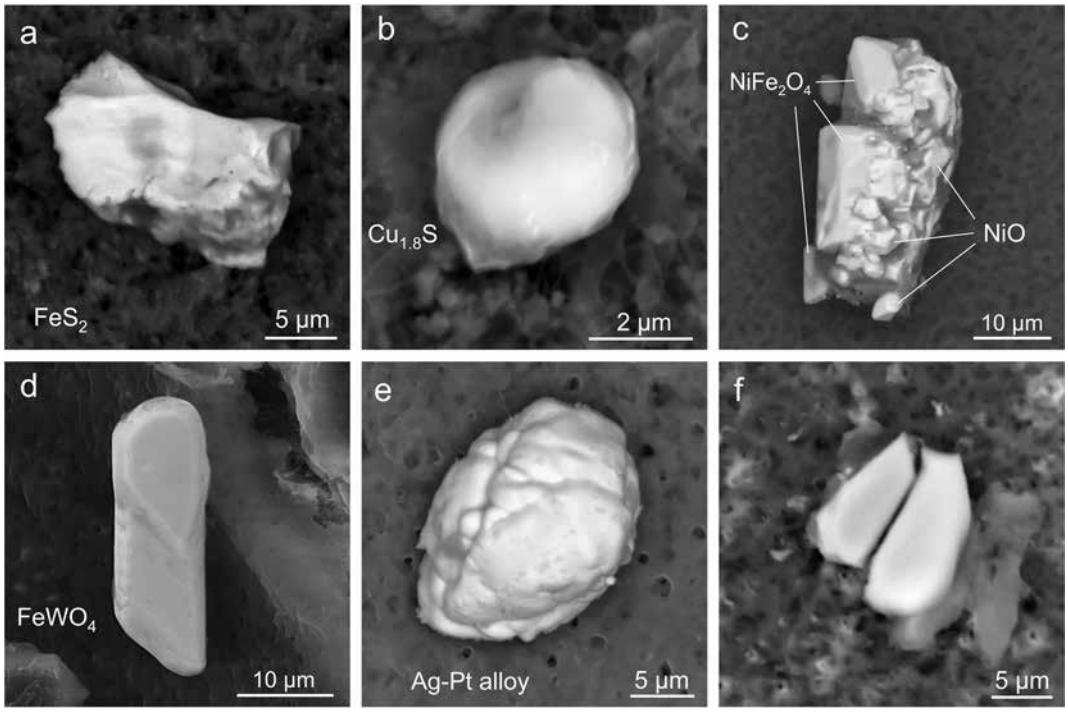

Figure 10. Aerosol particles of unclear origin. (a) Fragment of pyrite crystal (FeS_2). (b) Globule of digenite (Cu1.8S). (c) Aggregate of trevorite (Ni $(Fe,Ti)_2O_4$) and bunsenite (NiO) with remnants of silicate glass. (d) Crystal of ferberite ($Fe(W,Re)O_4$) containing 2 wt. % Re. (e) Globule of Ag-Pt alloy containing ~20 wt% Pt ($Ag_{0.88}Pt_{0.12}$). (f) Two fragments of titanite, $CaTiSiO_5$.

stained by small patches of silicate glass (Figure 10d). We included a 20-μm particle in the form of an irregular ellipsoid, consisting of an alloy of silver and platinum Ag80Pt20 (wt. %) or $Ag_{0.88}Pt_{0.12}$ (at. %), as an aerosol type of unclear genesis (Figure 10e). Only pyrite was relatively abundant, whereas chalcocite, ferberite, trevorite/bunsenite, and silver were represented by single particles. These minerals are typical in hydrothermal veins or supergene oxide zones of sulfide deposits and could originate from country rocks entrained by rising magma and fragmented in the course of the eruption.

2. Another group of unresolved aerosol particles comprises hollow magnetite spherules (Figure 11). Such spherules were notably abundant on filters and common in the fine fraction of the volcanic ash. The spherules have a black color and are composed of almost pure magnetite crystals with total contents of

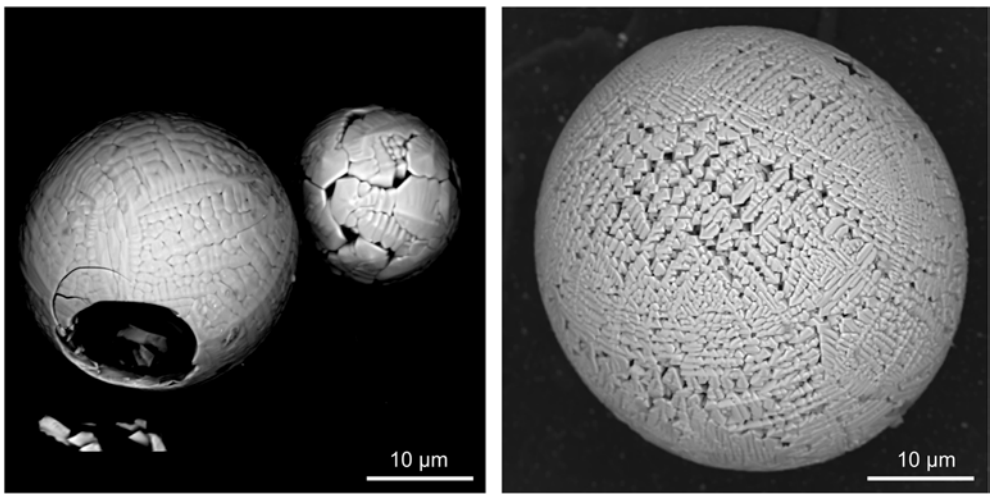

Figure 11. Hollow magnetite spherules.

S, Cr, Mn, Ti, Ni, and Cu not exceeding 0.5 wt. %. The size of the central cavity varies from approximately 50 to ~95% of the whole diameter. Such spherules were not observed to form aggregates with other aerosol minerals.

3. Phosphates and carbonates were sampled from the distal skylight, located ~1 km from the main crater, in the area where recent lava flows formed a shield more than 80 m thick (site 4 in Figures 1 and 2a). Blue fumes at a temperature of 120–150°C discharged from several open cracks ~20 cm wide. The collected particles included apatite, fluorite, chlor-spodiosite, calcite, some unidentified K-Ca carbonate, and Na-Ca carbonate, the latter with inferred Na:Ca ratio ~2 or a fine intergrowth of calcite and sodium carbonate. These phases occurred as single crystals 20–50 μm in size (Figure 12) or as aggregates (Figure 13). Some fluorite crystals contained apatite inclusions (Figure 12b), which may indicate pseudomorphs of fluorite after apatite. In addition to relatively large crystals of phosphates and fluorides, tiny particles of Ag_2S, native gold, and spherules of native iron were observed in such aggregates. Phosphates were not confined exclusively to this specific sampling site; rare particles of irregular shapes composed of Na-K and Al-Fe phosphate were present on filters collected at other sampling sites.

4.5. Comparison of Aerosol Captured at Different Degassing Vents

The Tolbachik aerosols collected at the various sampling sites vary in composition, such as in the ratio of nonsilicate to silicate components, including silicate microspheres. The largest amount of angular silicate particles and silicate microspheres was observed in samples from the active crater rim (sampling site 1; Figures 4a and 4c); forms such as Pele's hair were also present here (Figure 4c). Angular silicate particles were rare in other locations, but they were present in samples from all sampling sites. Most likely, such particles represent small fragments of tephra or solidified lava flows, carried by the winds.

The largest silicate microspheres, up to 64 μm in size, were observed on filters sampled from the plume over the large skylight in the lava tube roof (sampling site 2; Figure 4b). Microspheres were absent in aerosol samples from above the free surface of lava flow (sampling site 3) and in samples from the plume over cracks in the lava tube roof (sampling site 4). The presence of a cooled, viscous surficial layer on the lava flow is a probable explanation, since such a layer prevents bursts of small gas bubbles at the lava surface. The amount of H_2SO_4 droplets was the highest in the plume over the open-surface lava flow. Also, aerosols from above the surface of the lava flow contained more chlorides as compared to aerosols collected at sampling sites 1 and 2 upstream of the lava flow. This may result due to preferential SO_2 degassing from lava, while chlorine and fluorine are retained by silicate melt to be gradually released at distal parts of the lava flow.

The most intensive emission of condensation aerosol occurred from the large skylight (sampling site 2), where its content exceeded 90% by mass. The ratio between the main aerosol minerals at this site varied from ~90% Fe_2O_3 (Figure 7a) to ~90% $(Na, K)_2SO_4$ (Figure 7b). The highest flux of the condensation aerosol was observed at the sampling site 2 in February. Aerosols sampled in July from the plume over cracks in the lava tube roof consisted of rare single particles of nonsilicate minerals (Figures 12 and 13) and fragments of previously deposited sublimates (Figures 8g and 8h), with a low amount of condensation aerosol. Alteration aerosol was present mainly in samples taken from the plume over the large skylight (the sampling site 2) and also from the main crater. This reflects the conditions required for the formation of alteration aerosol: prolonged interaction of solid silicate rocks with high-temperature gases.

Overall, there was a decrease in degassing rate of lava with increase in distance from the main vent, as well as with time (decrease in the lava effusion rate). This evolution in distance and time corresponded to a gradual change in composition of aerosol according to the sequence: (1) angular silicate fragments, (2) silicate microspheres, (3) Na-K-Fe condensation aerosol and alteration aerosol, and (4) nonvolcanic particles and fragmented sublimates.

4.6. Thermodynamic Calculations vs. Observed Mineralogy of the Tolbachik Aerosol

The observed phase composition of aerosol is similar to the equilibrium composition of the gas-rock system over the temperature range of 600 to 900°C (Figure 14). The two most abundant aerosol phases, Na-K sulfate and Fe (III) oxide, were predicted by the model, with the disagreement that double Na-K sulfate was modeled as two separate sulfates. The occurrence of oxides and hydroxides and Ca-sulfate (anhydrite) in aerosol was also predicted by model calculations. The only large discrepancy between the model prediction and natural samples was the absence of $MgSO_4$ in the aerosol. According to the model, sulfates of alkali metals are

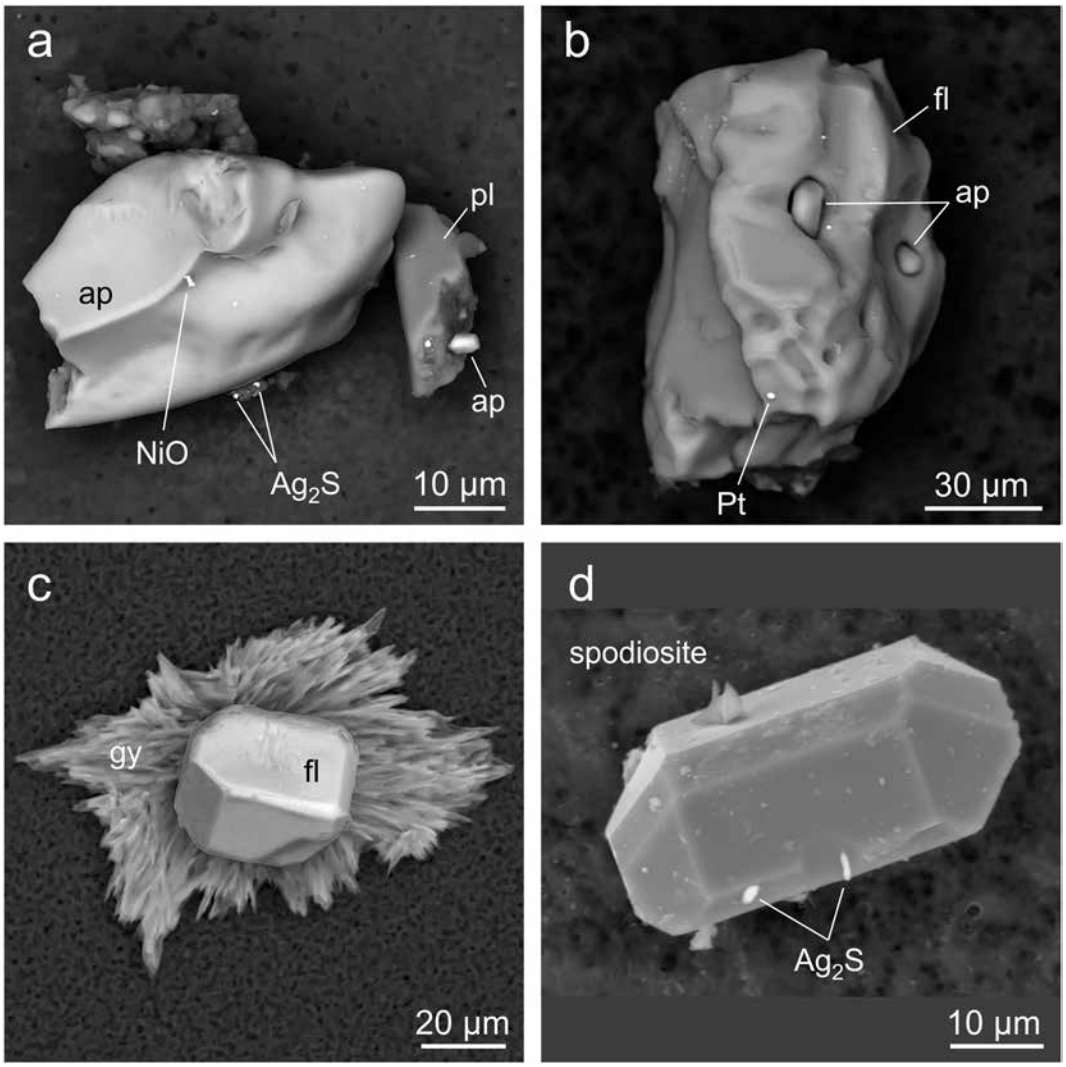

Figure 12. Phosphates and fluorite in aerosol emissions of Tolbachik. (a) Group of aerosol particles consisting of subhedral crystals of fluoroapatite (ap), plagioclase (pl) and rock fragment. Smaller particles of bunsenite (NiO) and acanthite (Ag_2S) attached to large apatite crystal. (b) Subhedral crystal of fluorite (fl) with two inclusions of subhedral fluoroapatite (ap) and several small platinum particles attached to fluorite. (c) Euhedral crystal of fluorite (fl) surrounded by fringe composed of secondary gypsum (gy); such secondary sulfates presumably formed due to interaction of sulfuric acid with Ca-rich minerals directly on filter. (d) Euhedral crystal of rare Ca phosphate chlor-spodiosite, Ca_2PO_4Cl (also called goryainovite; Ivanyuk et al., 2017), with particles of acanthite (Ag_2S) attached. Backscattered electron images.

stable between 600 and 900°C, but they transform into gaseous chlorides at higher temperatures. The model also predicts the specific high-temperature mineral assemblage, which consists of spinel (magnesioferrite and hercynite), magnetite, orthopyroxene and clinopyroxene, feldspathoids, and mullite. The Cu-bearing spinel was found in a thin crust covering the walls of the Tolbachik lava tube (Kamenetsky et al., 2019; Sharygin et al., 2018) and among aerosol particles (Figure 8k).

According to the model, sulfuric acid appears in the gaseous form below 700 and becomes the main sulfur species below 440°C (not shown in Figure 14). From approximately 300°C, gaseous H_2SO_4 begin to condense forming sulfuric acid aerosol; liquid H_2SO_4 dominates below 160°C. The modeling data reproduce well the observed speciation of solid aerosol and the presence of liquid H_2SO_4. The equilibrium model cannot predict the actual degree of SO_2 conversion to sulfates and sulfuric acid, since kinetics is responsible for this (Boreskov, 1954; Sander et al., 1984). A rough estimate of the mass ratio of sulfate aerosol deposited on a filter to the gaseous SO_2 pumped through the same filter gave value of $(Na,K)SO_4/SO_2 \approx 0.0075$. This ratio was calculated from Na, K, and SO_2 contents in the gas (Zelenski et al., 2014), and observations that more than

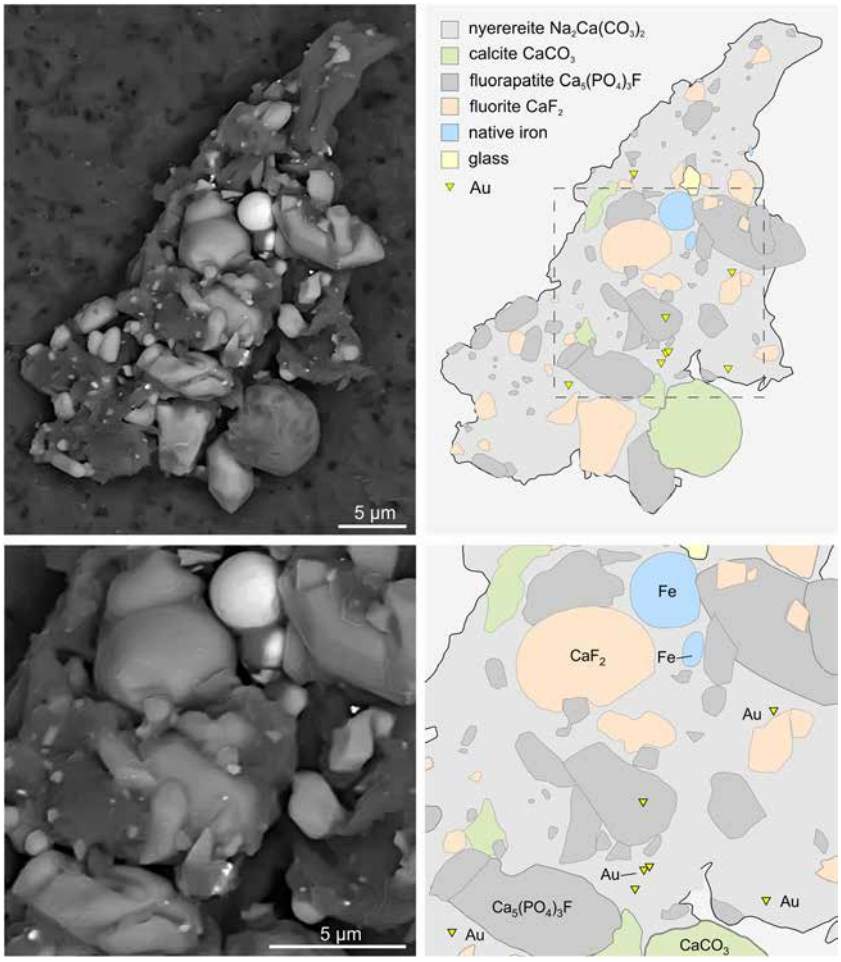

Figure 13. An aerosol particle composed of fluoroapatite, fluorite, Na- and Ca-carbonates, native iron, clasts of silicate glass and disseminated gold crystals.

90% of Na and K exist in the form of sulfate (this work). The conclusion is that for kinetic reasons, only a small fraction of SO_2 in the plume above the lava flow and skylights in the lava tube was converted to H_2SO_4. The latter immediately reacts with alkali metal chlorides present in the gas to form sulfate aerosol.

5. Discussion

5.1. Morphology as a Key to the Origin of Aerosol Particles

Tolbachik aerosols contain a large amount of the condensation aerosol. Particles of this type can condense directly from the gas phase (desublimation), can condense into a liquid phase with subsequent solidification upon cooling, and can precipitate on a solid surface (desublimation) with subsequent fragmentation. We argue that several morphological features indicate that the condensation of aerosol particles occurs directly from the gas phase, in contrast to minerals previously deposited on the rock surface and within cracks in the form of sublimates and subsequently fragmented. We deduce these features by comparing the morphology of Tolbachik aerosol particles and well-documented aerosols of different origins from industrial areas of China and India (e.g., Khafaie, 2013; Li et al., 2016; Xu et al., 2017, and references therein), including condensation aerosol (soot and fly ash), mineral and biogenic aggregates, and sea spray aerosol. Soot and fly ash particles are believed to result from gas-phase condensation during cooling of combustion products, whereas mineral and biogenic particles are mainly formed as a result of fragmentation.

Morphological evidence of condensation of aerosol particles directly from the gas include the following:

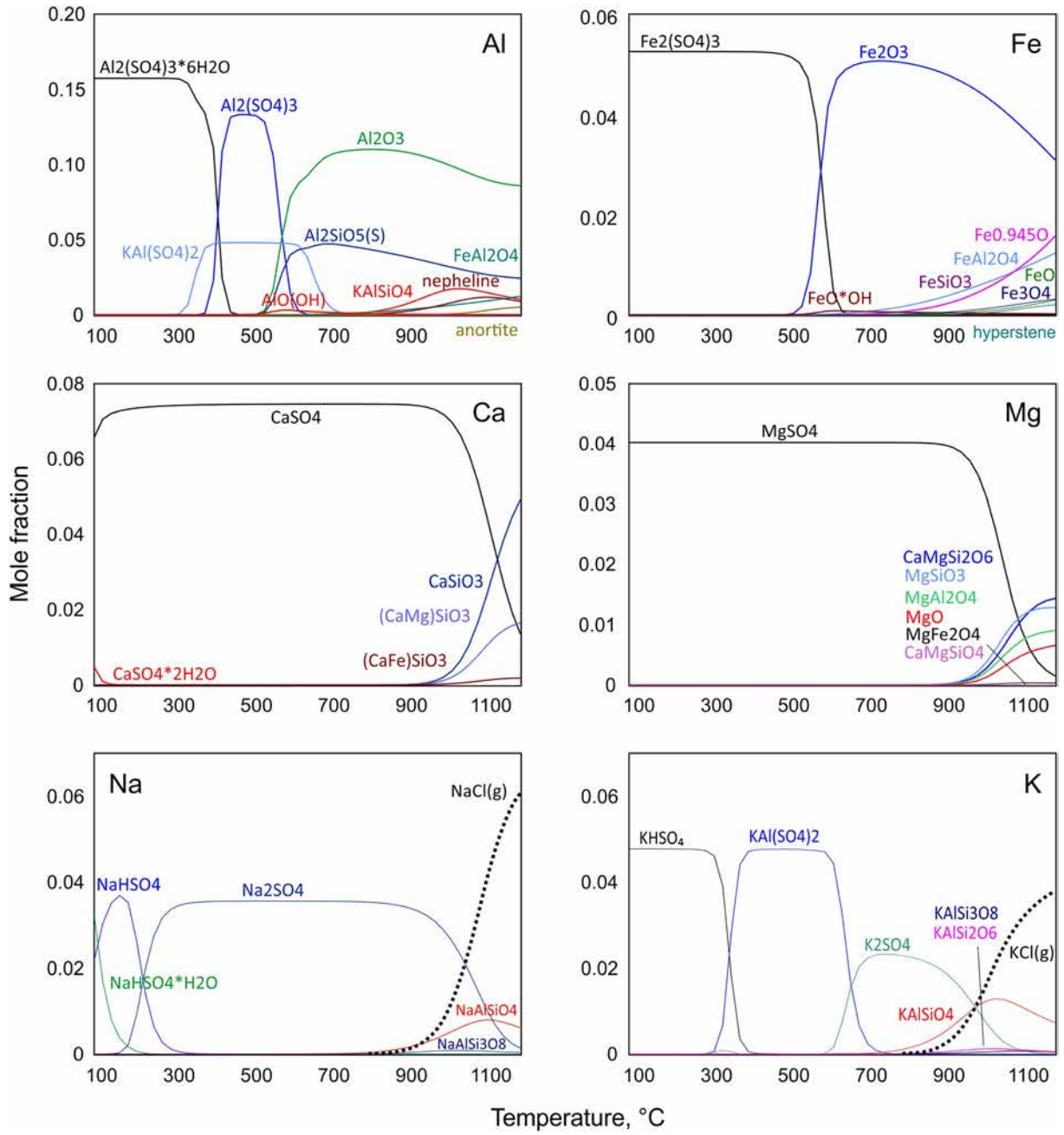

Figure 14. Temperature evolution of the gas-air system as derived from thermodynamic modeling based on the Outokumpu code HSC 6.1 Chemistry code and data base (Roine, 2007). The most abundant solid and gaseous species of Al, Fe, Ca, Mg, Na, and K are plotted. The chemical composition of the model system combines one mole of basalt with 100 moles of the volcanic gas of Tolbachik and 100 moles of air. Basaltic melt and basaltic glass were not considered among the possible phases because of unknown thermodynamic properties. Notwithstanding this fact, the observed composition of aerosol at the skylight closely resembles the calculated composition in the temperature range from 600 to 900°C, with several exceptions. The predicted, but not observed phase is $MgSO_4$, which was absent in the sampled aerosol. On the contrary, aluminum fluorides (ralstonite, $Na_xMg_xAl_{2-x}(F,OH)_6{\cdot}H_2O$, unnamed mineral $AlF_3{\cdot}nH_2O$) were observed, but not predicted by the model.

1. The crystals are single, not in aggregates (Figures 7a–7c and 7k).
2. The crystals have rounded (Figure 7b) or isometric shapes with clearly defined faces (Figures 7a and 7c).
3. The crystals are small, from hundreds nanometer to 2–5 μm in size (Figures 7a–7k).
4. Rounded, fluffy aggregates (Figures 7g and 7h).
5. Fractal-shaped aggregates (Figure 7d); such fluffy and fractal aggregates are composed of a single phase.

6. The best-known example of fluffy fractal-shaped aggregates grown directly from the gaseous phase is snow.

Indications that aerosol particles formed as a result of fragmentation of previously condensed mineral aggregates are the opposite of the characteristics listed above. Particles formed as a result of fragmentation of sublimates are represented by features including the following:

1. polycrystalline aggregates (Figures 8a–8k);
2. polymineralic aggregates (Figures 8a–e, 8h, and 8k);
3. aggregates with dense, nonporous texture (Figures 8a–8k);
4. large aerosol particles - tens of micrometers (Figures 8a–8k); and
5. aerosol particles with angular or irregular shape (Figures 8d, 8g, and 8k).

Some particles may share features characteristic of both crystals condensed directly from the gas and fragmented particles of preaerosol deposits on a substrate (Figures 7e and 7f). It is also possible that some particles with similar morphology are of different origin.

The spherical or roundish crystals of $(Na,K)_2SO_4$ (Figures 7a and 7b), in our opinion, are evidence that the condensation of the mineral occurred initially into the liquid, and crystals (aggregates) formed only after the liquid sulfate cooled below the solidification point, partially retaining the shape of the initial sulfate droplets. The Na_2SO_4-K_2SO_4 system has a minimum eutectic melting point of approximately 830°C at 20 mol. % K_2SO_4 (Rowe et al., 1972). The Na_2SO_4-K_2SO_4 system was liquid at the Tolbachik gas temperature of 1065°C over a large range of Na:K ratios. Only pure sodium sulfate has a melting point at 1071°C, slightly above the gas temperature. Sulfates are common phases in volcanic aerosol (e.g., Galindo et al., 1998; Allen et al., 2006; Martin et al., 2008; Moune et al., 2010; Sawyer et al., 2011). In particular, large (up to 50 μm) sulfate microspheres and dendrites, composed of such microspheres, were described in fumarolic incrustations of Erta-Ale volcano, where the presence of sulfate liquid is explained by a high gas temperature, 1084°C, which exceeded melting points of alkali sulfates (Zelenski et al., 2013). The relatively large sulfate crystals in the Tolbachik aerosol, a modal size of 2-3 μm (Figures 7a–7c), is likely due to relatively large residence time of gas in the lava tube, ranging from several seconds to several minutes (Section 4.1.3).

5.2. The Behavior of Aerosol Particles in the Environment, Depending on Their Mineral Composition

The emission of high-temperature gases from magma results in the selective extraction of significant amount of rare volatile elements (e.g., Nriagu, 1989; Hinkley et al., 1999; Mather et al., 2003; Zelenski et al., 2014, Mather, 2015, Ilyinskaya et al., 2017). After exsolution from magmas, volcanic gases form various condensation aerosols on cooling (Figures 2 and 7 and 8). Only a small fraction of volcanic aerosol settles near the emission source (Calabrese et al., 2011); most aerosol particles are transported by air streams over hundreds to thousands kilometers (e.g., von Glasow et al., 2009). Sooner or later, the condensation aerosol particles return to the ground, where they are involved in the geochemical cycle, with various effects on the environment (von Glasow et al., 2009; Calabrese et al., 2011; Mather, 2015, and references therein). The mineral composition of aerosol particles affects their behavior in the environment.

The main physical and chemical properties of aerosol minerals that determine their fate include solubility in water, hardness, density, and chemical reactivity. The solubility of aerosol minerals determines their stability in wet environments. Hardness and density determines the behavior of mineral particles during fluvial transport. Tolbachik aerosol contains both soluble minerals (e.g., sulfates and chlorides of alkali metals, copper, zinc, and cadmium) and insoluble (Fe_2O_3, AgCl, Ag_2S, Au) as well as minerals of different densities (in the range from ~1 to 19.3) and with a wide variety of other properties. A detailed discussion of the behavior of trace elements from aerosols in Earth's atmosphere and environment is beyond the scope of this article, but two typical examples of contrasting behavior of trace elements are given below.

The rare and toxic element thallium contained in Tolbachik gases (0.11 ppm; Zelenski et al., 2014) forms both readily soluble and insoluble compounds upon gas cooling. Soluble thallium is contained as a trace element in Na-K sulfate aerosol; insoluble compounds are TlI and (Ag,Tl)(Cl,Br,I) (Table 1). If soluble salts are dissolved by water, then insoluble particles may accumulate at the surface around the emission center. Snow

samples collected during the Tolbachik eruption contained a large amount of soluble thallium compounds (Malik et al., 2013). In the spring, this snow melted and thallium entered the ground water. At the same time, thallium iodide aggregates were found in volcanic ash samples collected near the 2013 eruptive cone 4 years after the end of the eruption (Figure 7f).

The other example is gold. For a spherical gold particle with a diameter of 200 nm, the sedimentation rate in still air is about 3 cm/hr, if we do not take into account coagulation with other aerosol particles. Such particles are only removed from the atmosphere by wet sedimentation (e.g., Seinfeld & Pandis, 1997; Uematsu et al., 1983), playing the role of nuclei for water droplets or ice crystals. Based on the total emission of SO_2 during the 2013 Tolbachik eruption, calculated from petrological data (1,700 kt), and the measured Au/SO_2 ratio of 6.8E−8 in volcanic gas (Zelenski et al., 2014), about 115 kg of gold was emitted with volcanic gases. Judging by data obtained during the present study, a significant portion of the emitted gold formed submicron aerosol particles, which were dissipated in Earth's atmosphere to be deposited elsewhere, far from the eruptive center by the process of wet sedimentation. Gold particles emitted by other volcanoes may behave similarly.

5.3. Thermodynamic Modeling in Aerosol Study

Equilibrium thermodynamics allows the study of multicomponent and multiphase systems that contain dozens of elements and that are composed of dozens to hundreds of possible phases (Belov, 2002; Chudnenko, 2010; Hack, 1996; Karpov et al., 2002). This can be applied to geological environments, such as metasomatic sequences, interaction of volcanic gas with country rocks, or deposition of fumarolic sublimates (Churakov et al., 2000; Symonds & Reed, 1993; Taran et al., 2000). Such systems are difficult to study experimentally and often difficult to measure accurately, but they can be studied using thermodynamic models. Nevertheless, the complete volcanic system comprising silicate melt, volcanic gas, solid basalt, and aerosol cannot be modeled at the current time, since thermodynamic properties of the melt components and silicate glass of basalt groundmass are not available (Belov, 2002; Belov & Trusov, 1998; Chudnenko, 2010). By means of thermodynamic modeling, we can calculate properties and behavior (e.g., condensation vs. cooling) only for a simplified system consisting of gas and solid crystalline phases.

In addition to the restrictions imposed by the modeling process itself, there are also kinetic limitations. Equilibrium modeling predicts only the final state of the system but is not able to estimate the time and way in which this state will be reached. For example, gas-phase reactions at temperatures above 1000°C proceed quickly (e.g., compilation of Babushok & Dakdancha, 1993) but the rate of a gas-rock reaction is limited by diffusion, a slow process. Despite all limitations, our thermodynamic model explains the observed mineral assemblages in volcanic environment and predicts their change along with the changing conditions. The most important (and new) result of the simulation is that the mineral compositions of both the condensation aerosol and alteration aerosol are close to the equilibrium state in the volcanic gas-air-basalt system.

The model predicts the presence of alkali sulfates simultaneously with calcium sulfate. Sodium and potassium gaseous chlorides that are the main species of Na and K above 1000°C (Figure 14) appear to be precursors for the formation of Na and K sulfate particles, with double Na-K sulfate being one of the main components of the condensation aerosol. Whereas Na-K sulfate condenses from the gas, calcium sulfates (both anhydrite $CaSO_4$ and gypsum $CaSO_4{\cdot}2H_2O$), and Mg and Al fluorides and hydroxides coat particles of volcanic glass. According to thermodynamic calculations, Ca, Mg, and Al should not occur in noticeable amounts in the gas. For example, the total amount of gaseous Ca compounds at 1000°C in the system is 7 orders of magnitude lower than the amount of solid substances containing Ca. Therefore, it can be assumed that Ca, Mg, and Al minerals coating silicate particles (Figure 6) formed directly on the surface of these particles due to gas-solid reactions.

The model also predicts that iron is largely present in the form of Fe (III) oxide but does not specify reactions leading to formation of this substance in the aerosol. The intermediate volatile compound may be volatile iron chlorides (formed as a result of the interaction between gaseous HCl with FeO and Fe_2O_3 containing in rock):

$$2FeO(rock) + 4\,HCl = 2FeCl_2 + 2H_2O; Fe_2O_3(rock) + 6HCl = 2FeCl_3 + 3H_2O;$$

with gaseous FeCl2 and $FeCl_3$ then converted to solid Fe (III) oxide, releasing molecular chlorine, which subsequently oxidizes SO_2 to SO_3:

$$2FeCl_3 + 3O_2 = 2Fe_2O_3 + 3\,Cl_2; Cl_2 + SO_2 + 2H_2O = H_2SO_4 + 2HCl.$$

In this set of reactions, iron chlorides may serve as intermediate compounds and at the same time a de facto catalyst for sulfur dioxide conversion to sulfuric acid. Gaseous iron chloride is not shown in the equilibrium diagram (Figure 14), but according to the calculations, approximately 0.03% of the total iron content is present as a volatile. Similar reactions with iron chloride may have formed molecular chlorine in fumarolic gases emitted from cooling scoria cones (Zelenski & Taran, 2012).

Thermodynamic modeling of high-temperature volcanic gases (e.g., Symonds et al., 1990; Bernard et al., 1990; Symonds et al., 1990; Symonds & Reed, 1993; Churakov et al., 2000; Taran et al., 2001) focused on the gas composition and precipitation of solids from the gas upon equilibrium cooling. Only Symonds and Reed (1993) paid much attention to thermochemical modeling of the rock composition in equilibrium with high-temperature volcanic gas. However, the authors considered the interaction of rock with reduced volcanic gas not diluted by air. According to the calculations by Symonds and Reed (1993), an equilibrium system with gas:rock ratio of 100:1 (i.e., the same proportion as is in our model) contains almost no secondary minerals, with the exception of tridymite and a small amount of hematite. The authors simulated the interaction of the gas and dacite, a more felsic rock, so the existence of excess silica in the form of tridymite is natural. Recent work on gas-rock interaction (e.g., Delmelle et al., 2018) does not consider much detail of thermodynamic models. Modeling using a modern database of thermodynamic data (Roine, 2007) shows that even in the case of a significant excess of volcanic gas, most rock-forming elements do not evaporate, but remain in the solid state. However, all rock-forming elements are involved in the formation of secondary minerals. Pyroxenes are the most common minerals of basalt but appear only at the highest temperatures of the calculated model. The thermodynamic model predicts the phase composition of the gas-rock system more accurately than some experimental works (e.g., $CaSO_4$-NaCl system; Ayris et al., 2013, 2014; Delmelle et al., 2018), although such experiments were conducted for a simplified system at a temperature much lower than that of the Tolbachik gases.

5.4. Nonvolcanic Minerals in Volcanic Aerosol

Nonvolcanic minerals (particles) of the Tolbachik volcanic aerosol refer primarily to their chemical composition. These particles are not fragments of magma or volcanic rocks and have not condensed from the volcanic gas. However, they arose due to the mechanical or thermal energy of magma during the eruption. The presence of completely foreign particles (industrial or mineral dust) was not recorded during this study. Thus, the description of nonvolcanic minerals in Tolbachik aerosol is justified from the volcanological point of view.

5.4.1. Hydrothermal Minerals Within Volcanic Aerosol

Abundant pyrite, a typical hydrothermal mineral, is incompatible with magmatic conditions in the Tolbachik aerosol, as well as other minerals typical of hydrothermal veins and supergene zones of sulfide deposits. These minerals of nonvolcanic origin could be trapped by rising magma from unknown hydrothermal mineralization in rocks of the Tolbachik basement. Country-rock fragments are rare in volcanic aerosols. For example, metamorphic minerals were detected in aerosol over the Popocatepetl volcano (Obenholzner et al., 2003). Zelenski et al. (2016) suggested that the ubiquitous presence of gold among lavas and pyroclastic rocks of Plosky Tolbachik could be caused by the assimilation of an epithermal gold deposit at depth.

The finding of a relatively large (20 μm) irregular spherule of Ag-Pt alloy is somewhat enigmatic. Tolbachik aerosol contained numerous fine particles of silver sulfide (Ag_2S and acanthite) and halides (Ag[Cl,Br,I] and chlorargyrite), both likely generated by gas condensation. This association is consistent with the composition of the Tolbachik volcanic gas, which contains considerable HCl and traces of H_2S. Although H_2S was not identified in Tolbachik gas emissions (the detection limit for H_2S was ~0.1 mmol/mol; Zelenski et al., 2014), even trace amounts of this species could result in the formation of silver sulfide. Silver is common in hydrothermal deposits but rarely occurs in volcanic or fumarolic environments. For example, although

fumarolic minerals at Tolbachik comprises more than 250 species, including >100 copper-containing minerals and abundant native gold (see Mindat.org for "Tolbachik"), silver minerals have not been reported (aside from one description of native silver at Tolbachikthat has never been confirmed; Glavatskikh & Trubkin, 2000). Most likely, the only reliable findings of volcanic silver are the fine globules of native silver in the basalts of Kilauea volcano (Li & Boudreau, 2019). Given the similarity of the chemical properties of copper and silver, native silver at Tolbachik could form from the partial oxidation of silver sulfides, as suggested for copper at Kilauea (Li & Boudreau, 2019). The presence of 20 wt.% Pt in the silver spherules is more difficult to explain because platinum is not common in hydrothermal deposits. However, trace Pt was detected in Tolbachik gas emissions, comprising less than 0.5 ppb in the total gas (Zelenski et al., 2014).

5.4.2. Magnetite Spherules

Hollow magnetite spherules (Figure 11) were abundant in the Tolbachik aerosol, but their origin remains unclear. The morphology and composition of the spherules suggest that they are nonvolcanic and may originate from one or several extraneous sources. The presence of industrial dust (e.g., Zajzon et al., 2013) is unlikely because of the remoteness of Kamchatka from continental industrial regions. The cosmic hypothesis (Del Monte et al., 1974; Folco & Cordier, 2015; Wittke et al., 2013) is also unlikely due to the fact that spherules do not contain nickel and/or troilite (Del Monte et al., 1975; Genge et al., 2017). The most likely hypothesis for the origin of the magnetite spherules is pyrite combustion in eruptive gases. Such combustion (Groves et al., 1987; Srinivasachar et al., 1990) forms similar hollow microspheres. According to these authors, pyrite decomposes at ~600°C, forming pyrrhotite FeS. The melting point of pure FeS is 1194°C, which is 130°C higher than the temperature of magmatic gas measured at Tolbachik (1065°C). Further pyrrhotite oxidation $FeS + 3/2\ O_2 = FeO + SO_2$ is highly exothermic ($\Delta H = -190$ kJ/mol O_2). The oxidation could occur only in the gas medium (hot gas-air mixture) since the magma temperature is insufficient and the reaction temperature is buffered by the high heat capacity of magma. The oxidation by air raises the temperature of the pyrrhotite particles beyond their melting point. In the first stage of oxidation, an oxysulfide melt Fe-O-S is formed, with a melting point below 1100°C. In the second stage, after the oxidation of the sulfide, exothermic formation of magnetite occurs ($\Delta H = -138$ kJ/mol Fe_3O_4). Further oxidation of magnetite to hematite is limited for kinetic reasons (Srinivasachar et al., 1990; Srinivasachar & Boni, 1989).

5.4.3. Phosphate-Fluorite-Carbonate Particles With Gold and Native Iron

The existence of an association of phosphate, fluorite, and carbonate minerals with gold and native iron minerals raises many questions, even though each of the listed minerals has been described elsewhere among products of volcanic activity in one form or another. The first class of minerals here are carbonates. Although CO_2 is the second most abundant species in volcanic gases, fumarolic carbonate minerals are rare because of their instability in the presence of HCl, SO_2 and other volcanic acid species (e.g., Balić-Žunić et al., 2016). Nevertheless, significant amounts of secondary carbonates are found on some volcanoes. The best example is the Icelandic volcano Surtsey, where calcite, together with fluorite, hydromagnesite, and sulfates, is a common mineral occurring mainly in lava tubes and as crusts on lavas under ambient atmospheric temperature conditions (Jakobsson et al., 2008). Calcite is also a common mineral in Etna's lava caves (Barone et al., 2015); sodium carbonates were also described among the fumarole incrustations of Vesuvius (Balić-Žunić et al., 2016, and references therein). Several carbonates, including calcite ($CaCO_3$), hydromagnesite ($Mg_5(CO_3)_4(OH)_2{\cdot}4H_2O$), dypingite ($Mg_5(CO_3)_4(OH)_2{\cdot}5H_2O$), and thermonatrite ($Na_2CO_3{\cdot}H_2O$), were described for low-temperature fumarole sublimates at Tolbachik (Serafimova & Vergasova, 1981; Vergasova & Filatov, 1993). At the volcano Oldoinyo Lengai, Tanzania, natrocarbonatite lavas formed due to the influence of dense CO_2-rich fluid, based on one hypothesis (Nielsen & Veksler, 2002).

Apatite is a common early accessory mineral of basalts and occurs at Tolbachik in the form of inclusions in magnetite (Figure 3c). More felsic volcanic rocks typically contain 0.2–0.3% accessory apatite (e.g., Nakamaru et al., 2000; Piccoli & Candela, 2002, and references therein). In intrusive bodies of calcium carbonatites, apatite is one of the main noncarbonate minerals (Simandl & Paradis, 2018). Pure phosphates have not been reported from fumarolic minerals but can form solid solutions with arsenates such as the rare mineral rhabdoborite, which is a complex borate-phosphate-arsenate found at Tolbachik (Pekov et al., 2018). Native iron is locally present in basic rocks reduced by sedimentary carbon (Bugl, Germany, Medenbach & El Goresy, 1982; Siberian traps, Ryabov et al., 1985; Kamenetsky et al., 2013; Disco Island, Ulff-Møller, 1990) and in layered intrusions and ophiolites (e.g., Muskox, Canada, Chamberlain et al.,

1965; Kachkanar, Ural Mountains, Borisenko et al., 1982). Native iron is also present in the mineral list of the second eruptive cone of Tolbachik (Vergasova & Filatov, 1993).

The unusual phenomenon here is the coexistence of phases in one place or as aggregates, shapes of crystals, inclusions of apatite in fluorite, and the presence of a rare phosphate mineral chlor-spodiosite (goryainovite). The key question is what process can account for the presence of all of these minerals together. Possibilities include (1) products of deep interaction of solidified lava with CO_2- and HF-rich fluids; (2) fragments of carbonate-rich xenoliths or (3) interaction of such xenoliths with basaltic lavas; (4) interaction of lava with organic matter, which could reduce iron oxide to native iron and, at the same time, provide phosphorus and carbonates (the latter being common in biomass fly ash); and (5) aerosols not associated with the volcanic eruption. Currently, none of these possibilities can explain the simultaneous occurrence of all phases observed, for example, in the aerosol particle shown in Figure 12. Hypothesis (4) appears preferable, even though sampling site #4 was located at an altitude of about 1,500 m asl, well above the boundary of local vegetation. However, the geometry of the lava flows and lava tubes on Tolbachik at the time of sampling at site #4 (early July 2013) was such that the flow of hot lava spread down and reached the shrub and grass zone. Lava moved through tubes everywhere except for the front of the lava flow. Air circulation in these lava tubes occurred upstream in the opposite direction to the lava flow due to "chimney effect." Thus, it is possible that small particles of biomass ash and other combustion products, up to 20–40 microns in size, may have entered the lava tube at the lava front; these would have been transported by the turbulent stream of hot air along the 4-km-long lava tube and subsequently discharged to the atmosphere at the sampling point.

The compositions of biomass ash are well studied. One of the most comprehensive data sets on the chemical and mineral compositions of biomass ash was presented in a review by Vassilev et al. (2013). According to this work, typical wood and woody biomass or herbaceous biomass ash contains (on average) 15–43 wt. % CaO, 11–27 wt. % K_2O, and 3.5–6.5 wt. % P_2O_5 as well as SiO_2, Al_2O_3, MgO, Fe_2O_3, Na_2O, TiO_2, and SO_3. Ashes have a large variety of mineral compositions, which differ depending on the biomass composition and combustion conditions. Among more than 180 minerals described in the ashes (Vassilev et al., 2013, and references therein), there are numerous phosphates including apatite, and carbonates including calcite, K-Ca carbonates, and the rare Na-Ca carbonate natrofairchildite $Na_2Ca(CO_3)_2$. Although fly ash does not contain fluorite, the latter is a common mineral of lava tubes (Jakobsson et al., 2008) and could also be formed through the interaction of calcite and apatite from ash with volcanic gases containing HF.

Apatite inclusions in fluorite (Figure 12b) can be evidence of incomplete substitution of fluorite for apatite. The presence of abundant small (100–500 nm) crystals of gold and Ag_2S on phosphate-carbonate aerosol particles (Figures 11 and 12) is consistent with their ubiquitous presence in products of the 2012–2013 Tolbachik eruption (Chaplygin et al., 2015; Zelenski et al., 2016). Any mineral or rock aggregate in contact with volcanic gas, especially within the lava tube, could be covered by scattered nano-size crystals of gold.

6. Conclusions

The 2012–2013 Tolbachik eruption was accompanied by strong emissions of volcanic aerosol from the eruptive crater, from skylights in the roof of lava tubes and from the surface of the more distant lava flow. Three main classes of aerosol were identified: (1) fragmented silicate melt, (2) fragmented altered silicate and nonsilicate rocks, and (3) condensed gaseous species. The relative role of each class varied depending on sampling locations and dates of sampling. Droplets of H_2SO_4 represented a liquid fraction of the condensation aerosol.

Fragmented silicate melt includes particles of quenched glass and small crystals of rock-forming minerals. Silicate microspheres were assigned to originate from bursting bubbles on the surface of lava flows. The fragmented rock particles were composed mainly of secondary minerals. Thermodynamic modeling showed that the main phases observed in the aerosols are the predicted equilibrium products of the [silicate aerosol-volcanic gas-air system] in the temperature range of 600–900°C.

The main components of the condensation aerosol, Na-K sulfate, and hematite account for >95 wt. %. In addition to the main phases, other phases include sulfides of Fe, Cu, Ag, and Re; oxides and hydroxides of Al, Fe, Cu, Zn, Mo, W, Te, Ta, and Zr; halides of Al, Mg, Na, K, Ca, Cd, Pb, Ag, and Tl; sulfates of Na, K, Pb, Ca, and Ba; and others. Micron to submicron particles of Au and Ag_2S were ubiquitous everywhere

on larger particles of any of the aerosol classes, and in samples taken at all four sampling points, consistent with previous observations. Relatively large particles of volcanic sublimates occurred on filters and were considered as a subclass of the condensation aerosol. Such particles probably formed in cracks and cavities of lava flows and were subsequently fragmented and ejected with the volcanic gases. The variety of mineral composition in the condensation aerosols reflects the complex trace element composition of volcanic gas and variability of the condensation conditions.

The aerosol also contains minerals that are not characteristic of the volcanic fumarole or eruption environment. The most abundant mineral of this class was pyrite, but some other hydrothermal minerals, such as digenite, ferberite, and native silver, were present. The most likely source is from hydrothermal veins in the volcanic basement or from deeper altered country rocks. The presence of hollow magnetite microspheres was assigned to combustion of pyrite crystals during the course of the eruption. Filters collected at the distal part of the lava tube contained phosphates, fluorite, carbonates, and native iron, exotic minerals for active volcanoes but similar to minerals associated with biomass fly ash, formed after incineration of wood/shrub/grass (phosphate-carbonate fraction), and modified by interaction with volcanic gases (which contributed fluorite and gold crystals). Vegetation at the front of the lava flows may have been the source of aerosols of such composition, with ash transported by the ascending flow of air through the lava tubes, which acted as chimneys.

Volcanic aerosol is one form of volcanic emission. Depending on the eruption mode and intensity of explosive activity, the mass fraction of the condensation aerosol varies from negligible, in the case of intense volcanic explosions and the emission of ash clouds, to predominant (nonexplosive nature of eruption, high temperature of the lava, and presence of lava tubes), and can result in a significant redistribution of elements between geological environments. The physical and chemical properties of minerals comprising aerosol will determine the subsequent behavior of aerosol particles in the environment.

Acknowledgments
AcknowledgementsWe thank Vasiliy Yaschuk for his logistical support, Natalia Malik for their help in collecting samples, and Aleksey Nekrasov for his analytical assistance. We are grateful to reviewers Jeffrey Hedenquist and Evgenia Ilyinskaya for valuable comments that significantly improved the manuscript. This study was supported by the Russian Science Foundation grant 16-17-10145. Supporting information (which contains raw analytical data) is available at Dryad repository with DOI https://doi.org/10.5061/dryad.51c59zw4p.

References

Aiuppa, A., Dongarra, G., Valenza, M., Federico, C., & Pecoraino, G. (2003). Degassing of trace volatile metals during the 2001 eruption of Etna. *Geophysical Monograph*, *139*, 41–54. https://doi.org/10.1029/139GM03

Allen, A. G., Baxter, P., & Ottley, C. (2000). Gas and particle emissions from Soufrière Hills Volcano, Montserrat, West Indies: Characterization and health hazard assessment. *Bulletin of Volcanology*, *62*(1), 8–19. https://doi.org/10.1007/s004450050287

Allen, A. G., Mather, T. A., McGonigle, A. J. S., Aiuppa, A., Delmelle, P., Davison, B., et al. (2006). Sources, size distribution, and downwind grounding of aerosols from Mount Etna. *Journal of Geophysical Research*, *111*, D10302. https://doi.org/10.1029/2005JD006015

Ayris, P. M., Delmelle, P., Cimarelli, C., Maters, E. C., Suzuki, Y. J., & Dingwell, D. B. (2014). HCl uptake by volcanic ash in the high temperature eruption plume: Mechanistic insights. *Geochimica et Cosmochimica Acta*, *144*, 188201. https://doi.org/10.1016/j.gca.2014.08.028

Ayris, P. M., Lee, A. F., Wilson, K., Kueppers, U., Dingwell, D. B., & Delmelle, P. (2013). SO2 sequestration in large volcanic eruptions: High-temperature scavenging by tephra. *Geochimica et Cosmochimica Acta*, *110*, 58–69. https://doi.org/10.1016/j.gca.2013.02.018

Babushok, V. I., & Dakdancha, A. N. (1993). Global kinetic parameters for high-temperature gas-phase reactions. *Combustion, Explosion and Shock Waves*, *29*(4), 464–489. https://doi.org/10.1007/BF00782974

Balić-Žunić, T., Garavelli, A., Jakobsson, S. P., Jónasson, K., Katerinopoulos, A., Kyriakopoulos, K., & Acquafredda, P. (2016). Fumarolic Minerals: An overview of active european volcanoes. In K. Nemeth (Ed.), *Updates in volcanology: From volcano modelling to volcano geology*, (pp. 267–322). Rijeka, Croatia: InTech. https://doi.org/10.5772/61961

Barone G., Mazzoleni P., & Priolo, G. (2015) Catalogo delle mineralizzazioni secondarie riscon-trate all'interno di alcune grotte vulcaniche etnee (A catalogue of the secondary mineralizations in some Etnean volcanic caves). In: Proceedings of XXII Congresso Nazionale di Speleologia "Condividere i dati", Sessione Documentatione – a1; 30 May– 2 June 2015; Pertosa-Auletta (SA). pp. 99–109.

Belousov, A. B., Edwards, B., Volynets, A. O., & Mel'nikov, D. V. (2015). Overview of the precursors and dynamics of the 2012–13 basaltic fissure eruption of Tolbachik Volcano, Kamchatka, Russia. *Journal of Volcanology and Geothermal Research*, *299*, 19–20. https://doi.org/10.1016/j.jvolgeores.2015.04.009

Belov, G. V. (2002). *Termodinamicheskoe modelirovanie: metody, algoritmy, programmy (Thermodynamic Simulation: Methods, Algorithms, Programs)*. Moscow: Nauchnyi Mir. (in Russian)

Belov, V., & Trusov, B. G. (1998). Influence of thermodynamic and thermochemical data errors on calculated equilibrium composition. *Berichte der Bunsengesellschaft für Physikalische Chemie*, *102*(12), 1874–1879. https://doi.org/10.1002/bbpc.19981021219

Bernard, A., Symonds, R. B., & Rose, W. I.(1990). Volatile transport and deposition of Mo, W and Re in high temperaturemagmatic fluids. *Applied Geochemistry*, *5*(3), 317–326. https://doi.org/10.1016/0883-2927(90)90007-R

Bombrun, M., Harris, A., Gurioli, L., Battaglia, J., & Barra, V. (2015). Anatomy of a Strombolian eruption: Inferences from particle data recorded with thermal video. *Journal of Geophysical Research: Solid Earth*, *120*, 2367–2387. https://doi.org/10.1002/2014JB011556

Boreskov, G. K. (1954). *Catalysis in sulfuric acid production*. Moscow-Leningrad: GosKhimIzdat. (in Russian)

Borisenko, L. F., Begizov, V. D., & Kurilenko, N. M. (1982). Native iron in ore-olivinites of Kachkanarskii massif. *Doklady Akademii Nauk SSSR*, *264*, 947–950.

Calabrese, S., Aiuppa, A., Allard, P., Bagnato, E., Bellomo, S., Brusca, L., D'Alessandro, W. & Parello, F. (2011). Atmospheric sources and sinks ofvolcanogenic elements in a basaltic volcano (Etna, Italy). *Geochimicaet Cosmochimica Acta*, *75*(23), 7401–7425. https://doi.org/10.1016/j.gca.2011.09.040

Chamberlain, J. A., McLeod, C. R., Traill, R. J., & Lachance, C. R. (1965). Native metals in the Muskox intrusion. *Canadian Journal of Earth Sciences*, *2*(3), 188–215. https://doi.org/10.1139/e65-017

Chaplygin, I. V., Yudovskaya, M. A., Vergasova, L. P., & Mokhov, A. (2015). Native gold from volcanic gases at Tolbachik 1975–76 and 2012–13 Fissure Eruptions, Kamchatka. *Journal of Volcanology and Geothermal Research*, *307*, 200–209. https://doi.org/10.1016/j.jvolgeores.2015.08.018

Chudnenko, K. V. (2010). *Thermodynamic modeling in geochemistry: Theory, algorithms, software, application*, (p. 287). Novosibirsk, Russia: Academic Publishing House Geo. (in Russian)

Churakov, S. V., Tkachenko, S. I., Korzhinskii, M., Bocharnikov, R. E., & Shmulovich, K. I. (2000). Evolution of composition of high-temperature fumarolic gases from Kudryavy Volcano, Iturup, Kuril Islands: the thermodynamic modeling. *Geochemistry International*, *38*(5), 436–451.

Cook, W. R. (1972). Phase changes in Cu_2S as a function of temperature, in *Proceedings of 5th Materials Research Symposium*, *NBS Special Publication 364, Solid State Chemistry* (pp. 703–712). Washington, DC: National Bureau of Standards.

Crowe, B. M., Finnegan, D. L., Zoller, W. H., & Boynton, W. V. (1987). Trace element geochemistry of volcanic gases and particles from 1983–1984 eruptive episodes of Kilauea Volcano. *Journal of Geophysical Research*, *92*(B13), 13,708–13,714. https://doi.org/10.1029/JB092iB13p13708

Darzi, M. (1981). Fumarolic aerosols from Kilauea volcano, Hawaii. *Nuclear Instruments and Methods*, *181*(1–3), 359–365. https://doi.org/10.1016/0029-554X(81)90636-4

Del Monte, M., Nanni, T., & Tagliazucca, M. (1974). Origin of the cavities in black magnetic spherules. *Journal of Geophysical Research*, *79*(29), 4375–4378. https://doi.org/10.1029/jb079i029p04375

Del Monte, M., Nanni, T., & Tagliazucca, M. (1975). Ferromagnetic volcanic particulate matter and black magnetic spherules: A comparative study. *Journal of Geophysical Research*, *80*(14), 1880–1884. https://doi.org/10.1029/jb080i014p01880

Delmelle, P., Wadsworth, F. B., Maters, E. C., & Ayris, P. M. (2018). High Temperature Reactions between Gases and AshParticles in Volcanic Eruption Plumes. *Reviews in Mineralogy andGeochemistry*, *84*(1), 285–308. https://doi.org/10.2138/rmg.2018.84.8

Edmonds, M., Mather, T. A., & Liu, E. J. (2018). A distinct metal fingerprint in arc volcanic emissions. *Nature Geoscience*, *11*, 790–794. https://doi.org/10.1038/s41561-018-0214-5

Filatov, S. K., Shablinskii, A. P., Vergasova, L. P., Saprikina, O. Y., Bubnova, R. S., Moskaleva, S. V., & Belousov, A. B. (2018). Belomarinaite, IMA 2017-069a. CNMNC Newsletter No. 43, June 2018, page 781. *Mineralogical Magazine*, *82*, 779–785.

Folco, L., & Cordier, C. (2015). Micrometeorites. *European Mineralogical Union Notes in Mineralogy*, *15*, 253–297. https://doi.org/10.1180/EMU-notes.15.9

Galindo, I., Ivlev, L. S., González, A., & Ayala, R. (1998). Airborne measurements of particle and gas emissions from the December 1994-January 1995 eruption of Popocatépetl volcano (Mexico). *Journal of Volcanology and Geothermal Research*, *83*(3–4), 197–217. https://doi.org/10.1016/S0377-0273(98)00033-X

Gauthier, P., Sigmarsson, O., Gouhier, M., Haddadi, B., & Moune, S. (2016). Elevated gas flux and trace metal degassing from the 2014–2015 fissure eruption at the Bárðarbunga volcanic system, Iceland. *Journal of Geophysical Research: Solid Earth*, *121*, 1610–1630. https://doi.org/10.1002/2015JB012111

Genge, M. J., Davies, B., Suttle, M. D., van Ginneken, M., & Tomkins, A. G. (2017). The mineralogy and petrology of I-type cosmic spherules: Implications for their sources, origins and identification in sedimentary rocks. *Geochimica et Cosmochimica Acta*, *218*, 167–200. https://doi.org/10.1016/j.gca.2017.09.004

Glavatskikh, S. F., & Trubkin, N. V. (2000). Pervyye nakhodki samorodnykh volframa i serebra v produktakh eksgalyatsiy Bolshogo treshchinnogo Tolbachinskogo izverzheniya (Kamchatka) [First findings of native tungsten and silver in exhalation products of the Tolbachik Great Fissure Eruption, Kamchatka]. *Doklady Earth Sciences*, *373*(4), 523–526.

Gramaccioli, C. M., & Campostrini, I. (2007). Demartinite, a new natural polymorph of K2SiF6 from La Fossa crater, Vulcano, Aeolian Islands, Italy. *Canadian Mineralogist*, *45*, 1275–1280. https://doi.org/10.2113/gscanmin.45.5.1275

Groves, S. J., Williamson, J., & Sanyal, A. (1987). Decomposition of pyrite during pulverized coal combustion. *Fuel*, *66*(4), 461–466. https://doi.org/10.1016/0016-2361(87)90148-7

Hack, K. (Ed) (1996). *The SGTE casebook: thermodynamics at work*. London: Institute of Materials.

Hinkley, T. K., Lamothe, P. J., Wilson, S. A.,Finnegan, D. L., & Gerlach, T. M. (1999). Metal emissions from Kilauea, anda suggested revision of the estimated worldwide metal output by quiescentdegassing of volcanoes. *Earth and Planetary Science Letters*, *170*(3), 315–325. https://doi.org/10.1016/S0012-821X(99)00103-X

Huie, R. (1986). *Chemical kinetics of intermediates in the autoxidation of SO2*, in *Fossil Fuels Utilization Series*, vol. 319, Markuszewski R. & Blaustein, B. D. (Eds.) (pp. 284–292). Washington, DC: American Chemical Society. https://doi.org/10.1021/bk-1986-0319.ch023

Ilyinskaya, E., Martin, R. S., & Oppenheimer, C. (2012). Aerosol formation in basaltic lava fountaining: Eyjafjallajökull volcano, Iceland. *Journal of Geophysical Research*, *117*, D00U27. https://doi.org/10.1029/2011JD016811

Ilyinskaya, E., Oppenheimer, C., Mather, T. A., Martin, R. S., & Kyle, P. R. (2010). Size-resolved chemical composition of aerosol emitted by Erebus volcano, Antarctica. *Geochemistry, Geophysics, Geosystems*, *11*, Q03017. https://doi.org/10.1029/2009GC002855

Ilyinskaya, E., Schmidt, A., Mather, T. A., Pope, F. D., Witham, C., Baxter, P., et al. (2017). Understanding the environmental impacts of large fissure eruptions: Aerosol and gas emissions from the 2014–2015 Holuhraun eruption (Iceland). *Earth and Planetary Science Letters*, *472*, 309–322. https://doi.org/10.1016/j.epsl.2017.05.025

Ivanyuk, G. Y., Yakovenchuk, V. N., Pakhomovsky, Y. A., Panikorovskii, T. L., Konoplyova, N. G., Bazai, A. V., et al. (2017). Goryainovite, Ca_2PO_4Cl, a new mineral from the Stora Sahavaara iron ore deposit (Norrbotten, Sweden). *Journal of the Geological Society of Sweden*, *139*(1), 75–82. https://doi.org/10.1080/11035897.2016.1227363

Jakobsson, S. P., Leonardsen, E. S., & Balić-Žunić, T. (2008). Encrustations from three recent volcanic eruption in Iceland: The 1963-1967 Surtsey, 1973 Eldfell and the 1991 Hekla eruptions. *Fjölrit*, *52*, 1–65.

Kamenetsky, V. S., Belousov, A. B., Sharygin, V. V., Zhitova, L. M., Ehrig, K., Zelenski, M. E., et al. (2019). High-temperature gold-copper extraction with chloride flux in lava tubes of Tolbachik volcano (Kamchatka). *Terra Nova*, *31*(6), 511–517. https://doi.org/10.1111/ter.12420

Kamenetsky, V. S., Charlier, B., Zhitova, L., Sharygin, V., Davidson, P., & Feig, S. (2013). Magma chamber-scale liquid immiscibility in the siberian traps represented by melt pools in native iron. *Geology*, *41*(10), 1091–1094. https://doi.org/10.1130/G34638.1

Karpov, I. K., Chudnenko, K. V., Kulik, D. A., & Bychinskii, V. A. (2002). The convex programming minimization of five thermodynamic potentials other than Gibbs energy in geochemical modeling. *American Journal of Science*, *302*(4), 281–311. https://doi.org/10.2475/ajs.302.4.281

Khafaie, M. A. (2013) A study to evaluate the plausible mechanism of air pollution effect on diabetes. Ph. D. thesis.
Kondratyev, K., Ivlev, L., Krapivin, V. F., & Varotsos, C. (Eds) (2006). *Atmospheric Aerosol Properties: Formation, Processes and Impacts*. Berlin: Springer-Praxis.
Lefèvre, R., Gaudichet, A., & Billon-Galland, M. (1986). Silicate microspherules intercepted in the plume of Etna volcano. *Nature*, *322*(6082), 817–820. https://doi.org/10.1038/322817a0
Li, P., & Boudreau, A. E. (2019). Vapor transport of silver and gold in basaltic lava flows. *Geology*, *47*(9), 877–880. https://doi.org/10.1130/g46407.1
Li, W., Shao, L., Zhang, D., Ro, C. U., Hu, M., Bi, X., et al. (2016). A review of single aerosol particle studies in the atmosphere of EastAsia: Morphology, mixing state, source, and heterogeneous reactions. *Journalof Cleaner Production*, 112(January 2013), 1330–1349. https://doi.org/10.1016/j.jclepro.2015.04.050
Malik, N. A., Zelenski, M. E., & Okrugin, V. M. (2013). Emission of elements by eruptive gases of Tolbachik, 2013. In: *Materials of the conference "Volcanism and related processes"*, Petropavlovsk-Kamchatsky: IVS FEB RAS.
Martin, R. S., Mather, T. A., Pyle, D. M., Power, M., Allen, A. G., Aiuppa, A., et al. (2008). Composition-resolved size distributions of volcanic aerosols in the Mt. Etna plumes. *Journal of Geophysical Research*, *113*, D17211. https://doi.org/10.1029/2007JD009648
Martin, R. S., Mather, T. A., Pyle, D. M., Power, M., Tsanev, V. I., Oppenheimer, C., et al. (2009). Size distributions of fine silicate and other particles in Masaya's volcanic plume. *Journal of Geophysical Research*, *114*, D09217. https://doi.org/10.1029/2008JD011211
Martin, R. S., Sawyer, G. M., Day, J. A., Leblond, J. S., Ilyinskaya, E., & Oppenheimer, C. (2012). High-resolution size distributions and emission fluxes of trace elements from Masaya volcano, Nicaragua. *Journal of Geophysical Research*, *117*, B08206. https://doi.org/10.1029/2012JB009487
Mather, T. A. (2015). Volcanoes and the environment: Lessons for understanding Earth's past and future from studies of present-day volcanic emissions. *Journal of Volcanology and Geothermal Research*, *304*, 160–179. https://doi.org/10.1016/j.jvolgeores.2015.08.016
Mather, T. A., Oppenheimer, C., Allen, A. G., & McGonigle, A. J. S. (2004). Aerosol chemistry of emissions from three contrasting volcanoes in Italy. *Atmospheric Environment*, *38*(33), 5637–5649. https://doi.org/10.1016/j.atmosenv.2004.06.017
Mather, T. A., Pyle, D. M., & Oppenheimer, C. (2003). *Tropospheric volcanic aerosol*. *Geophysical Monograph Series*, 139, 189–212. https://doi.org/10.1029/139GM12
Mather, T. A., Tsanev, V. I., Pyle, D. M., McGonigle, A. J. S., Oppenheimer, C., & Allen, A. G. (2004). Characterization and evolution of tropospheric plumes from Lascar and Villarrica volcanoes, Chile. *Journal of Geophysical Research*, *109*, D21303. https://doi.org/10.1029/2004JD004934
Mather, T. A., Witt, M. L. I., Pyle, D. M., Quayle, B. M., Aiuppa, A., Bagnato, E., et al. (2012). Halogens and trace metal emissions from the ongoing 2008 summit eruption of Kīlauea volcano, Hawaii. *Geochimica et Cosmochimica Acta*, *83*, 292–323. https://doi.org/10.1016/j.gca.2011.11.029
Medenbach, O., & El Goresy, A. (1982). Ulvöspinel in native iron-bearing assemblages and the origin of these assemblages in basalts from Ovifak, Greenland, and Buhl, Federal Republic of Germany. *Contributions to Mineralogy and Petrology*, *80*, 358–366. https://doi.org/10.1007/BF00378008
Meeker, G., & Hinkley, T. K. (1993). The structure and composition of microspheres from the Kilauea volcano, Hawaii. *American Mineralogist*, *78*, 873–876.
Meeker, K., Chuan, R. L., Kyle, P. R., & Palais, J. (1991). Emission of elemental gold particles from Mount Erebus, Ross Island, Antarctica. *Geophysical Research Letters*, *18*(8), 1405–1408. https://doi.org/10.1029/91GL01928
Menard, G., Moune, S., Vlastélic, I., Aguilera, F., Valade, S., Bontemps, M., & González, R. (2014). Gas and aerosol emissions from Lascar volcano (Northern Chile): Insights into the origin of gases and their links with the volcanic activity. *Journal of Volcanology and Geothermal Research*, *287*, 51–67. https://doi.org/10.1016/j.jvolgeores.2014.09.004
Moune, S., Gauthier, P. J., & Delmelle, P. (2010). Trace elements in the particulate phase of the plume of Masaya Volcano, Nicaragua. *Journal of Volcanology and Geothermal Research*, *193*(3–4), 232–244. https://doi.org/10.1016/j.jvolgeores.2010.04.004
Nakamaru, Y., Nanzyo, M., & Yamasaki, S. (2000). Utilization of apatite in fresh volcanic ash by pigeonpea and chickpea. *Soil Science and Plant Nutrition*, *46*(3), 591–600. https://doi.org/10.1080/00380768.2000.10409124
Nielsen, T. F., & Veksler, I. V. (2002). Is natrocarbonatite a cognate fluid condensate? *Contributions to Mineralogy and Petrology*, *142*(4), 425–435. https://doi.org/10.1007/s004100100306
Nriagu, J. O. (1989). A global assessment ofnatural sources of atmospheric trace metals. *Nature*, *338*, 47–49. https://doi.org/10.1038/338047a0
Obenholzner, J. H., Schroettner, H., & Delgado, H. (2003). Particles from the plume of Popocatépetl volcano, Mexico - The FESEM/EDS approach. *Geological Society Special Publication*, *213*, 123–148. https://doi.org/10.1144/GSL.SP.2003.213.01.08
Okrugin, V., Favero, M., Liu, A., Etschmann, B., Plutachina, E., Mills, S., et al. (2017). Smoking gun for thallium geochemistry in volcanic arcs: Nataliyamalikite, TlI, a new thallium mineral from an active fumarole at Avacha Volcano, Kamchatka Peninsula, Russia. *American Mineralogist*, *102*(8), 1736–1746. https://doi.org/10.2138/am-2017-6057
Pekov, I. V., Zubkova, N. V., Koshlyakova, N. N., Belakovskiy, D. I., Vigasina, M. F., Agakhanov, A. A., et al. (2018). Rhabdoborite-(W), IMA 2017-109. CNMNC Newsletter No. 42, April 2018. *Mineralogical Magazine*, *82*, 445–451.
Pekov, I. V., Zubkova, N. V., Yapaskurt, V. O., Belakovskiy, D. I., Chukanov, N. V., Lykova, I. S., et al. (2014). Wulffite, $K_3NaCu_4O_2(SO_4)_4$, and parawulffite, $K_5Na_3Cu_8O_4(SO_4)_8$, two new minerals from fumarole sublimates of the Tolbachik Volcano, Kamchatka, Russia. *Canadian Mineralogist*, *52*, 699–716. http://doi.org/10.3749/canmin.1400018
Piccoli, P. M., & Candela, P. A. (2002). Apatite in igneous systems, Phosphates: Geochemical, geobiological and material importance. In M. J. Kohn, J. Rakovan, & J. M. Hughes (Eds.), *Reviews in Mineralogy and Geochemistry*, (Vol. 48, pp. 255–292). Washington, DC: Mineralogical Society of America. https://doi.org/10.2138/rmg.2002.48.6
Plechov, P. Y., Blundy, J. D., Nekrylov, N., Melekhova, E., Shcherbakov, V. D., & Tikhonova, M. S. (2015). Petrology and volatile content of magmas erupted from Tolbachik Volcano, Kamchatka, 2012–13. *Journal of Volcanology and Geothermal Research*, *307*, 182–199. https://doi.org/10.1016/j.jvolgeores.2015.08.011
Pollard, F. H., Hanson, P., & Nickless, G. (1961). Chromatographic studies on the oxidation of sulphurous acid by ferric iron in aqueous acid solution. *Journal of Chromatography A*, *5*, 68–73. https://doi.org/10.1016/S0021-9673(01)92817-1
Roine, A. (2007), HSC chemistry 6.1, Tech. Rep., Outotec Research Oy. Pori, Finland.
Rowe J.J. Zen L.S., Morey G.W. (1972). *The quinary reciprocal salt system Na, K, Mg, Ca/Cl, SO4. A review of literature with new data*, *Professional Paper* (Vol. 741, 1–44). Washington, DC: Geology Survey.
Ryabov, V. V., Pavlov, A. L., & Lopatin, G. G. (1985). *Native Iron of the Siberian Traps*. Novosibirsk, Russia: Nauka Publisher. (In Russian)

Sander, U. H. F., Fischer, H., Rothe, U., & Kola, R. (1984). *Sulphur, sulphur dioxide and sulphuric acid*, (1st ed.). London: The British Sulphur Corporation Limited.

Sawyer, G. M., Salerno, G. G., Le Blond, J. S., Martin, R. S., Spampinato, L., Roberts, T. J., et al. (2011). Gas and aerosol emissions from Villarrica volcano, Chile. *Journal of Volcanology and Geothermal Research*, *203*(1–2), 62–75. https://doi.org/10.1016/j.jvolgeores.2011.04.003

Seinfeld, J. H., & Pandis, S. N. (Eds) (1997). *Atmospheric chemistry and physics: From air pollution to climate change*. New York: Wiley-VCH.

Serafimova, E. K., & Vergasova, L. P. (1981). On the formation of hydromagnesite on lava flows from Tolbachik volcano eruption in 1975–1976. *Doklady Akademii Nauk SSSR*, *259*, 680–683. (in Russian)

Sharygin, V. V., Kamenetsky, V. S., Zhitova, L. M., Belousov, A. B., & Abersteiner, A. (2018). Copper-containing magnesioferrite in vesicular trachyandesite in a lava tube from the 2012–2013 Eruption of the Tolbachik Volcano. *Minerals*, *8*(11), 514. https://doi.org/10.3390/min8110514

Simandl, G. J., & Paradis, S. (2018). Carbonatites: related ore deposits, resources, footprint, and exploration methods. *Applied Earth Science: Transactions of the Institute of Mining and Metallurgy*, *127*(4), 123–152. https://doi.org/10.1080/25726838.2018.1516935

Spadaro, F., Leferve, R., & Ausset, P. (2002). Experimental rapid alteration of basaltic glass: Implications for the origins of atmospheric particulates. *Geology*, *30*(8), 671–674. https://doi.org/10.1130/0091-7613(2002)030<0671:ERAOBG>2.0.CO;2

Srinivasachar, S., & Boni, A. A. (1989). A kinetic model for pyrite transformations in a combustion environment. *Fuel*, *68*, 829–836. https://doi.org/10.1016/0016-2361(89)90116-6

Srinivasachar, S., Helble, J. J., & Boni, A. A. (1990). Mineral behavior during coal combustion 1. Pyrite transformations. *Progress in Energy and Combustion Science*, *16*(4), 281–292. https://doi.org/10.1016/0360-1285(90)90037-4

Symonds, R. B., & Reed, M. H. (1993). Calculation of multicomponent chemical equilibria in gas-solid-liquid systems: calculation methods, thermochemical data, and applications to studies of high-temperature volcanic gases with examples from Mount St. Helens. *American Journal of Science*, *293*, 758–864. https://doi.org/10.2475/ajs.293.8.758

Symonds, R. B., Reed, M. H., & Rose, W. I.(1992). Origin, speciation, and fluxes of trace-element gases at Augustinevolcano, Alaska: Insights into magma degassing and fumarolic processes. *Geochimicaet Cosmochimica Acta*, *56*(2), 633–657. https://doi.org/10.1016/0016-7037(92)90087-Y

Symonds, R. B., Rose, W. I., Reed, M. H.,Lichte, F., & Finnegan, D. L. (1987). Volatilization, transport andsublimation of metallic and non-metallic elements in high temperature gases atMerapi Volcano, Indonesia. *Geochimica et Cosmochimica Acta*, *51*(8),2083–2101. https://doi.org/10.1016/0016-7037(87)90258-4

Taran, Y. A., Bernard, A., Gavilanes, J. C., & Africano, F. (2000). Native gold in mineral precipitates from high-temperature volcanic gases of Colima volcano, Mexico. *Applied Geochemistry*, *15*(3), 337–346. https://doi.org/10.1016/S0883-2927(99)00052-9

Taran, Y. A., Bernard, A., Gavilanes, J.-C.,Lunezheva, E., Cortes, A., & Armienta, M. A. (2001). Chemistry andmineralogy of high-temperature gas discharges from Colima volcano, Mexico. Implicationsfor magmatic gas–atmosphere interaction. *Journal of Volcanology andGeothermal Research*, *108*(1–4), 245–264. https://doi.org/10.1016/S0377-0273(00)00289-4

Telling, J., Flower, V. J. B., & Carn, S. A. (2015). A multi-sensor satellite assessment of SO_2 emissions from the 2012–13 eruption of Plosky Tolbachik volcano, Kamchatka. *Journal of Volcanology and Geothermal Research*, *307*, 98–106. https://doi.org/10.1016/j.jvolgeores.2015.07.010

Uematsu, M., Duce, R. A., Prospero, J. M., Chen, L., Merrill, J. T., & McDonald, R. L. (1983). Transport of mineral aerosol from Asia over the North Pacific Ocean. *Journal of Geophysical Research*, *88*(C9), 5343–5352. https://doi.org/10.1029/JC088iC09p05343

Ulff-Møller, F. (1990). Formation of native iron in sediment-contaminated magma: I. A case study of the Hanekammen Complex on Disko Island, West Greenland. *Geochimica et Cosmochimica Acta*, *54*(1), 57–70.https://doi.org/10.1016/0016-7037(90)90195-q

Varekamp, J. C., Thomas, E., Germani, M., & Buseck, P. R. (1986). Particle geochemistry of volcanic plumes of Etna and Mount St. Helens. *Journal of Geophysical Research*, *91*(B12), 12,233–12,248. https://doi.org/10.1029/JB091iB12p12233

Vassilev, S. V., Baxter, D., Andersen, L. K., & Vassileva, C. G. (2013). An overview of the composition and application of biomass ash. Part 1. Phase-mineral and chemical composition and classification. *Fuel*, *105*, 40–76. https://doi.org/10.1016/j.fuel.2012.09.041

Vergasova, L. P., & Filatov, S. K. (1993). Minerals of volcanic exhalations—A new genetic group (after the data of Tolbachik volcano eruption in 1975–1976). *Proceedings of the Russian Mineralogical Society*, *1993*(4), 68–76.

Vergasova, L. P., & Filatov, S. K. (2012). New mineral species in products of fumarole activity of the Great Tolbachik fissure eruption. *Journal of Volcanology and Seismology*, *6*, 281–289. https://doi.org/10.1134/S0742046312050053

Volynets, A. O., Edwards, B. R., Mel'nikov, D. V., Yakushev, A., & Griboedova, I. (2015). Monitoring of the volcanic rock compositions during the 2012–2013 fissure eruption at Tolbachik volcano, Kamchatka. *Journal of Volcanology and Geothermal Research*, *307*(1), 120–132. https://doi.org/10.1016/j.jvolgeores.2015.07.014

von Glasow, R., Bobrowski, N., & Kern, C. (2009). The effects of volcanic eruptions on atmospheric chemistry. *Chemical Geology*, *263*, 131–142. https://doi.org/10.1016/j.chemgeo.2008.08.020

Willeke, K., & Baron, P. A. (Eds) (1993). *Aerosol measurement: Principles, techniques and applications*. New York, USA: Van Nostrand Reinhold.

Wittke, J. H., Weaver, J. C., Bunch, T. E., Kennett, J. P., Kennett, D. J., Moore, A. M. T., et al. (2013). Evidence for deposition of 10 million tonnes of impact spherules across four continents 12,800 y ago. *Proceedings of the National Academy of Sciences of the United States of America*, *110*, E2088–E2097. https://doi.org/10.1073/pnas.1301760110

Xu, L., Liu, L., Zhang, J., Zhang, Y., Ren, Y., Wang, X., & Li, W. (2017). Morphology, composition, and mixing state of individual aerosolparticles in Northeast China during wintertime. *Atmosphere*, *8*(3). https://doi.org/10.3390/atmos8030047

Zajzon, N., Márton, E., Sipos, P., Kristály, F., Németh, T., Kis-kovács, V., & Weiszburg, T. G. (2013). Integrated mineralogical and magnetic study of magnetic airborne particles from potential pollution sources in industrial-urban environment. *Carpathian Journal of Earth and Environmental Sciences*, *8*(1), 179–186. http://real.mtak.hu/id/eprint/41300

Zelenski, M. E., Fischer, T. P., de Moor, J. M., Marty, B., Zimmermann, L., Ayalew, D., et al. (2013). Trace elements in the gas emissions from the Erta Ale volcano, Afar, Ethiopia. *Chemical Geology*, *357*, 95–116. https://doi.org/10.1016/j.chemgeo.2013.08.022

Zelenski, M. E., Kamenetsky, V. S., & Hedenquist, J. (2016). Gold recycling and enrichment beneath volcanoes: A case study of Tolbachik, Kamchatka. *Earth and Planetary Science Letters*, *437*, 35–46. https://doi.org/10.1016/j.epsl.2015.12.034

Zelenski, M. E., Malik, N., & Taran, Y. A. (2014). Emissions of trace elements during the 2012–2013 effusive eruption of Tolbachik volcano, Kamchatka: enrichment factors, partition coefficients and aerosol contribution. *Journal of Volcanology and Geothermal Research*, *285*, 136–149. https://doi.org/10.1016/j.jvolgeores.2014.08.007

Zelenski, M. E., & Taran, Y. A. (2012). Volcanic emissions of molecular chlorine. *Geochimica et Cosmochimica Acta*, *87*, 210–226. https://doi.org/10.1016/j.gca.2012.03.034

Zoller, W. H., Parrington, J., & Phelan Kotra, J. (1983). Iridium enrichment in airborne particles from Kilauea volcano: January 1983. *Science*, *222*, 4–7. http://www.sciencemag.org/content/222/4628/1118.short

Zreda-Gostynska, G., Kyle, P. R., Finnegan, D. L., & Prestbo, K. M. (1997). Volcanic gas emissions from Mount Erebus and their impact on the Antarctic environment. *Journal of Geophysical Research*, *102*(B7), 15,039–15,055. https://doi.org/10.1029/97JB00155